ZAMM · Z. angew. Math. Mech. **72** (1992) 2, 113 – 132 Akademie Verlag

SEND, W.

The Mean Power of Forces and Moments in Unsteady Aerodynamics

Die Bilanz für die mechanische Energie dient als Ausgangspunkt für eine einheitliche und konsistente Darstellung der beiden grundlegenden und der instationären Aerodynamik innewohnenden Mechanismen Vortrieb und Flattern. Beide Erscheinungen hängen wechselseitig voneinander ab und sind gegeneinander austauschbar allein durch die Veränderung der reduzierten Frequenz als der beherrschenden Größe bezüglich instationärer Effekte.

The balance of mechanical energy serves as the starting point for a unified and consistent approach to the two basic and inherent mechanisms in unsteady aerodynamics, propulsion and flutter. Both phenomena are mutually dependent and interchangeable with each other by a mere variation of the reduced frequency as the governing magnitude with respect to unsteady effects.

Баланс для механической энергии служит отправной точкой для единого и состоятельного представления обоих основных и внутренных нестационарной аэродинамики механизмов – вторжение и флаттер. Оба феномены являются попарно зависимыми и взаимозаменяемыми только при помощи изменения приведенной частоты являющей преобладающей величиной относительно нестационарных эффектов.

MSC (1980): 76B05

1. Introduction

According to P. BUBLITZ [1] in his thorough survey of the history of aeroelasticity the very first experiments in unsteady aerodynamics were carried out by R. KATZMAYR [2] in 1922. In context with the propulsion of birds Katzmayr investigates the mean lift and thrust of three profiles belonging to the Göttingen series Gnnn, where nnn denotes a 3-digit number [3]. The profiles selected closely resemble the wing cross-sections of medium-sized birds like pigcons (cf. G189 and a typical aerofoil section in [4], p. 70, 71). The results of Katzmayr's experiments show that a pure plunging motion, despite a slight increase in drag and decrease in lift, leaves the steady polar curve unchanged, whereas pure pitching motion causes a drastic increase in drag for increasing pitch amplitudes. Thus the lift decreases for a positive steady angle of incidence and increases for a negative angle. To the author's knowledge, Katzmayr's measurements were never interpreted theoretically. In addition to other conclusions, the results will be explained in the course of this paper. A series of theoretical papers appears in the field of unsteady aerodynamics in the two decades following Katzmayr's experiments, almost all of them predict thrust for pure plunging motion or try to explain the phenomenon of propulsion from the point of view of quasi-steady aerodynamics. Neither the experimental results denying precisely these predictions are regarded nor is the crucial test repeated, if doubts about the reliability of the data occurred.

In 1924 unsteady aerodynamics is founded with W. BIRNBAUM's famous paper [5] in which he already states that "propulsion requires necessarily a nonzero plunging motion in combination with a pitching motion delayed by approximately 90° versus the plunge" (p. 285). However, he also predicts, that "even pure plunging motion produces thrust similar to the Knoller-Betz effect", whereas Katzmayr finds an increase in the drag coefficient.

In 1936 H. G. KÜSSNER [6] postulates an efficiency $\eta = -u_0 W_m / L_m \geqq 0.5$ of the pure plunging motion for any reduced frequency, where η is the ratio of the mean propulsive power $-u_0 W_m$ to the mechanically raised energy L_m to maintain the plunging motion. He explains the origin of the formula (in the right hand column of p. 418) as follows:

Each line of bound vorticity experiences a force perpendicular to the direction of the flow passing the line. Since the air along the plate does not flow precisely in the horizontal x-direction, the aerodynamic force must possess a small horizontal component, which is compared to the lift in the order of magnitude of the angle of incidence. This component is the induced drag, which may become negative for a suitable plunging motion of the aerofoil, that means, it may produce a propulsive force.

Küssner applies the well known analogy between force $\boldsymbol{F} = \Gamma \, \Delta \boldsymbol{r} \times \varrho \boldsymbol{v}_{\mathrm{kin}}$ acting on a vortex line of strength Γ and length $\Delta \boldsymbol{r}$, which passes a fluid at rest with the kinematic velocity $\boldsymbol{v}_{\mathrm{kin}}$, and force $\boldsymbol{F}_e = I \, \Delta \boldsymbol{r} \times \boldsymbol{B}$ on a steady electric current of strenght I and length $\Delta \boldsymbol{r}$ in a steady magnetic field $\boldsymbol{B}$. Of course, the formula predicts the right lift. But the analogy also holds truc for the next step, in which the powers are to be computed. The two forces are powerless forces, i.e. no energy is required to exert the forces. The expression for the mechanical power $P = \boldsymbol{F} \cdot \boldsymbol{v}_{\mathrm{kin}}$ thus vanishes for the same reason as the electric power ($I \, \Delta \boldsymbol{r}$ may be considered the flow $e \boldsymbol{v}_e$ of a continuous stream of electric charges e).

In contradiction to this conclusion, the propulsive force of an oscillating aerofoil requires continuous mechanical energy to overcome the loss of energy carried away by the disturbed particles (enriched with kinetic energy in the boundary layer) or – expressed differently – contained in the trailing vortices.

Though I. E. GARRICK [7], also focussing his paper on "the propelling or drag force experienced in a uniform airstream by an airfoil", computes very carefully the energy content of the wake, he obtains results similar to Birnbaum and Küssner: "It is observed that a propelling force exists in the entire range of l/k, the efficiency being 50 percent for

infinitely rapid oscillations and 100 percent for infinitely slow flapping" ([7], p. 425; k is equal to ω^*). Including TH. THEORDORSEN's work [8] and H. WAGNER's explanation for the lift of an impulsively starting aerofoil [9], the classical papers [5] to [9] have formed the basis of unsteady aerodynamics up to now. The computations of lift and moment for the oscillating aerofoil (including the aileron) and their successful application to flutter analysis experienced extensions into three dimensions, compressible flow and non-harmonic motion. Nevertheless the following presentation and discussion of a newly formulated approach to propulsion and flutter does not necessarily require an exhaustive review of all the papers subsequently published and frequently referring to the above mentioned classical authors.

2. The mean power

Considered is a rigid body passing through a fluid with the prescribed velocity $\boldsymbol{v}$. To maintain the motion a force $\boldsymbol{F}$ continuously supports the moving body to balance the force $\boldsymbol{F}_{\text{fluid}} = -\boldsymbol{F}$ resulting from the fluid (e.g. for an aeroplanc the thrust of the engine compensates for the frictional force). Work W done by force $\boldsymbol{F}$ acting on the body passing distance $\mathrm{d}\boldsymbol{r}$ during time interval $\mathrm{d}t$ is

$$W = \int \boldsymbol{F} \cdot \mathrm{d}\boldsymbol{r} = \int \boldsymbol{F} \cdot \boldsymbol{v}\, \mathrm{d}t \quad \text{with} \quad \boldsymbol{v} := \frac{\mathrm{d}\boldsymbol{r}}{\mathrm{d}t} \tag{1}$$

or

$$W = \int \boldsymbol{F}_{\text{fluid}} \cdot \mathrm{d}\boldsymbol{r}_{\text{kin}} = \int \boldsymbol{F}_{\text{fluid}} \cdot \boldsymbol{v}_{\text{kin}}\, \mathrm{d}t \tag{1a}$$

with $\boldsymbol{v}_{\text{kin}}$ describing the kinematic motion of the fluid relative to the moving body. The integrand in the second expression for W is the rate of working, in other words the power

$$P(t) = \boldsymbol{F}(t) \cdot \boldsymbol{v}(t) \quad \text{or} \quad P(t) = \boldsymbol{F}_{\text{fluid}}(t) \cdot \boldsymbol{v}_{\text{kin}}(t)\,. \tag{2}$$

For harmonic variations of the kinematic velocity, this expression leads to the key equation of the paper, the mean power $\langle P \rangle$ during the period T of the oscillations

$$\langle P \rangle = \frac{1}{T} \int_0^T P(t)\, \mathrm{d}t\,. \tag{3}$$

The concept provides a unified and consistent approach to the basic and inherent mechanisms in unsteady aerodynamics, propulsion and flutter. Both mechanisms are to be seen as complementary features in the different degrees of freedom; they are mutually dependent and interchangeable with each other by a mere variation of the reduced frequency ω^*, based on half chord length $l/2$ and the undisturbed onset velocity u_0,

$$\omega^* := \frac{\omega \cdot l/2}{u_0}\,, \tag{4}$$

where $\omega = 2\pi/T$ is the circular frequency of the harmonic oscillation. ω^* is the governing magnitude with respect to unsteady effects in acrodynamics. For a dynamic system with n degrees of freedom, represented by the generalized coordinates q_f, the mean power consists of the n individual contributions $\langle P_f \rangle$

$$\langle P \rangle = \sum_{f=1}^{n} \langle P_f \rangle = \sum_{f=1}^{n} \langle Q_f \cdot \dot{q}_f \rangle\,, \tag{5}$$

with Q_f as the generalized forces and $\dot{q}_f := \mathrm{d}q_f/\mathrm{d}t$ as the generalized velocities. Each $\langle P_f \rangle$ may change its sign depending on the various parameters in the mechanical system. The sign means

$\langle P_f \rangle > 0$ Power is consumed (has to be provided for the system),

$\langle P_f \rangle < 0$ Power is produced (has to be released from the system).

However, the total mean power is expected to remain positive, since it balances the kinetic energy gained by the fluid in the wake.

3. The kinematic velocity field

The mechanical system is a streamlined obstacle starting impulsively with a prescribed velocity $\boldsymbol{v}$ at a distinct time and surrounded by a sufficiently large volume of fluid which is assumed to be completely at rest before the motion starts. Hence, the content of kinetic energy in the fluid is zero before the motion begins. Attached to the space containing the fluid is a frame of reference $B = \{o; \boldsymbol{e}_1, \boldsymbol{e}_2, \boldsymbol{e}_3\}$ with o as the origin and $\{\boldsymbol{e}_i\}$ as the vector basis derived from the natural

Cartesian coordinates (x^i) in the sense of $\boldsymbol{e}_i := \partial/\partial x^i$. The notation with respect to differential geometry follows [10] throughout the paper. Particularly the Einstein summation convention holds; expressions like (x^i) are to be read as (x^1, x^2, x^3) and terms like $x^i E_i^j$ mean $x^1 \cdot E_1^j + x^2 \cdot E_2^j + x^3 \cdot E_3^j$. The lower index i in E_i^j denotes the rows and the upper index j the columns of the matrix $\underline{E} = ((E_i^j))$. Another frame of reference $B^* = \{o^*; \boldsymbol{e}_1^*, \boldsymbol{e}_2^*, \boldsymbol{e}_3^*\}$ with o^* as the comoving origin and the basis $\{\boldsymbol{e}_j^*\}$ derived from the Cartesian coordinates (x^{*j}) fixed with the blade (Figure 1) permits the precise description of the obstacle's motion.

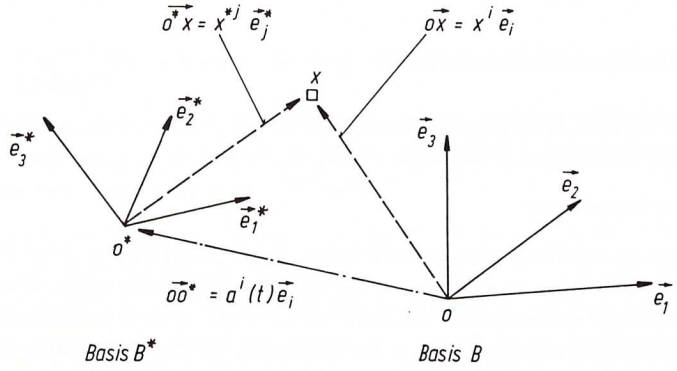

Fig. 1. Space-fixed and comoving coordinate systems

Any point x in the space may be located either with respect to B by the vector $\overrightarrow{ox} = x^i \boldsymbol{e}_i$ or with respect to B^* by the vector $\overrightarrow{o^*x} = x^{*j}\boldsymbol{e}_j^*$, briefly expressed by $\boldsymbol{x}$ and $\boldsymbol{x}^*$. The transformation from B to B^* is effected by translation of the origin $\overrightarrow{oo^*} = a^i(t)\,\boldsymbol{e}_i$ and orthogonal rotation of the vector basis $\boldsymbol{e}_j^* = E_j^i(t)\,\boldsymbol{e}_i$ with the determinant of the transformation matrix $\underline{E}$ being $\det(\underline{E}) = +1$ and $\underline{E}^{-1} = \underline{E}^T$. The transformation is uniquely defined by the functions $a^i(t)$ and $E_j^i(t)$. Of course, one or more transformations may follow one another, each of which in general consists of one translation plus one rotation. For the one transformation from B to B^* considered here the two alternative descriptions of an arbitrary point x lead to the following formulas for the transformations between the two coordinate systems

$$x^i(x^{*j}, t) = a^i(t) + x^{*j}E_j^i(t) \quad \text{and} \quad x^{*j}(x^i, t) = (x^i - a^i(t))\,E_i^{Tj}(t)\,. \tag{6}$$

Two different kinematic velocity fields which have to be distinguished very carefully follow from Eq. (6). The first one is $\boldsymbol{v}_{\text{kin,B}}$ and describes the rate of change with respect to time of the (x^i), if the (x^{*j}) are kept fixed

$$\boldsymbol{v}_{\text{kin,B}}^i(x^{*j}, t) := \frac{\partial}{\partial t}\,[x^i(x^{*j}, t)]_{x^{*j}} = \dot{a}^i(t) + x^{*j}\dot{E}_j^i(t)\,. \tag{7}$$

The field describes the motion of the moving body (the $\boldsymbol{v}$ in Eq. (1)). The second kinematic velocity field is designated $\boldsymbol{v}_{\text{kin,B*}}^*$ and describes the rate of change with respect to time of the (x^{*j}), if the (x^i) are kept fixed

$$v_{\text{kin,B*}}^{*j}(x^i, t) := \frac{\partial}{\partial t}\,[x^{*j}(x^i, t)]_{x^i} = -\dot{a}^i(t)\,E_i^{Tj}(t) + (x^i - a^i(t))\,\dot{E}_i^{Tj}(t)\,. \tag{8}$$

This last field is the very one which describes the apparent kinematic velocity of the fluid with respect to a comoving observer. Besides the different physical meanings, the components of the two vector fields are given with respect to different bases and the first one may not be used for the inner product with a force computed in the comoving frame without transformation of the components. Replacing the coordinates (x^{*j}) in Eq. (7) and (x^i) in Eq. (8) by the respective terms in Eq. (6), the components of $\boldsymbol{v}_{\text{kin,B}}(\boldsymbol{x}, t)$ are

$$v_{\text{kin,B}}^i(x^k, t) = \dot{a}^i(t) + (x^k - a^k(t))\,E_k^{Tj}(t)\,\dot{E}_j^i(t) \tag{9}$$

and for $\boldsymbol{v}_{\text{kin,B*}}^*(\boldsymbol{x}^*, t)$

$$v_{\text{kin,B*}}^{*j}(x^{*k}, t) = -\dot{a}^{*j}(t) - x^{*k}\Omega_k^{Tj}(t)\,; \qquad \dot{a}^{*j}(t) := \dot{a}^k(t)\,E_k^{Tj}(t) \tag{10}$$

and

$$\Omega_k^{Tj}(t) := -E_k^i(t)\,\dot{E}_i^{Tj}(t)\,, \quad \text{with} \quad \underline{\Omega} = \underline{E} \cdot \dot{\underline{E}}^T = -\underline{\Omega}^T\,. \tag{11}$$

The antisymmetric matrix $\underline{\Omega}$ is frequently called the matrix of rotation. If $\boldsymbol{v}_{\text{kin,B}}$ is transformed into the basis B^* by $\boldsymbol{v}_{\text{kin,B}}^* = \underline{E} \cdot \boldsymbol{v}_{\text{kin,B}}$ the components of the two fields may be compared. The preceding transformation reads explicitly

$$v_{\text{kin,B}}^{*j} = v_{\text{kin,B}}^i \cdot E_i^{Tj} = \dot{a}^i \cdot E_i^{Tj} + (x^k - a^k)\,E_k^{Tl}\dot{E}_l^i \cdot E_l^{Tj}\,. \tag{12}$$

With Eq. (6) and $\dot{\underline{E}} \cdot \underline{E}^T = (\underline{E} \cdot \dot{\underline{E}}^T)^T = \underline{\Omega}^T$ the final result is

$$v_{\text{kin,B}}^{*j} = \dot{a}^{*j}(t) + x^{*l}\Omega_l^{Tj}(t)\,. \tag{13}$$

With respect to the same vector basis the two kinematic velocity fields differ merely by a sign $\boldsymbol{v}^*_{\text{kin, B}} = -\boldsymbol{v}^*_{\text{kin, B*}}$. The only field of further interest is now $\boldsymbol{v}^*_{\text{kin, B*}}$, referred to simply as $\boldsymbol{v}^*_{\text{kin}}$.

The field above enters the integral equation for the solution of the flow problem which determines the relative velocity field $\boldsymbol{v}^*_{\text{rel}} = \boldsymbol{v}^*_{\text{ind}} + \boldsymbol{v}^*_{\text{kin}}$ of the fluid particles relative to the obstacle. $\boldsymbol{v}^*_{\text{ind}}$ is the physical motion of the fluid (with respect to the space); in classical aerodynamics the field is induced by the "weak" boundary condition which requires a vanishing normal component of the relative velocity for all points on the surface of the obstacle. A closer discussion of the physical approximations leading to this integral equation may be found in [11], [12].

4. No propulsion by a pure plunging motion in linearized theory

For a pure plunging motion, the transformation B into B^* with the translation $(a^i(t)) = (-g(t), 0, -h(t))$, $g(t) = u_0 t$, $h(t) = h_0 \cos \omega t$, and the trivial rotation $\underline{E} = \text{diag}\,(1, 1, 1)$, Eq. (10) yields

$$(v^{*j}_{\text{kin}}(x^{*k}, t)) = (\dot{g}(t), 0, \dot{h}(t)) = (u_0, 0, -h_0\omega \sin \omega t)\,. \tag{14}$$

The conventions for the motion are the usual ones in unsteady aerodynamics; the airfoil starts at $t = 0$ "at the bottom" and moves "from the right to the left". Once the kinematics is defined, the amplitudes and phase shifts (obtained from the real and imaginary parts) of the unsteady forces and moments are uniquely determined relative to the motion and, of course, within the limits of the theory. As a consequence of the theory, a harmonically varying kinematic velocity field leads to harmonically varying forces and moments. Without knowing further details, the force $\boldsymbol{F}^*$ ($\equiv \boldsymbol{F}^*_{\text{fluid}}$) resulting from Eq. (14) may be described in 2D theory by

$$(F^{*j}(t)) = (\bar{F}_{x,h} \cos(\omega t + \phi_{x,h}), 0, \bar{F}_{z,h} \cos(\omega t + \phi_{z,h}))\,. \tag{15}$$

$\bar{F}_{x,h}$, $\bar{F}_{z,h}$ are the amplitudes and $\phi_{x,h}$, $\phi_{z,h}$ the phase shifts versus $h(t)$ yielding the power

$$P(t) = F^{*j}(t) \cdot v^{*l}_{\text{kin}}(t) \cdot \boldsymbol{e}^*_j \cdot \boldsymbol{e}^*_l \quad \text{with} \quad \boldsymbol{e}^*_j \cdot \boldsymbol{e}^*_l = \delta_{jl} = \begin{cases} 1 \text{ for } j = l \\ 0 \text{ for } j \neq l \end{cases}. \tag{16}$$

With Eqs. (14) and (15) $P(t)$ in the previous formula reads explicitly

$$P(t) = u_0 \cdot \bar{F}_{x,h} \cos(\omega t + \phi_{x,h}) - h_0\omega \sin \omega t \cdot \bar{F}_{z,h} \cos(\omega t + \phi_{z,h}) \tag{17}$$

and leads to the mean power according to Eq. (3)

$$\langle P \rangle = +\tfrac{1}{2} h_0\omega \cdot \bar{F}_{z,h} \sin \phi_{z,h}\,. \tag{18}$$

BIRNBAUM [5] gives a "rough approximation" for the mean negative drag $-\langle D \rangle$ of a plunging motion, which reads in the notation of this paper

$$-\langle D \rangle = F_0 \cdot 2\pi\omega^{*2} \left(\frac{h_0}{l/2}\right)^2 \quad \text{with} \quad F_0 := q_0 \cdot S\,, \qquad q_0 := \frac{1}{2} \varrho u_0^2\,, \tag{18a}$$

where h_0 is the plunge amplitude, ω^* the reduced frequency based on half chord length $l/2$, ϱ the density of the fluid, u_0 the undisturbed onset velocity and $S = lb$ the surface with b as the span. Küssner proves that the approximate formula (18a) for the trust of the pure plunging motion in Birnbaum's paper holds true for all reduced frequencies (W_m in Eq. (55) of [6]). The reduced frequency in Katzmayr's experiment is about $\omega^* \cong 0.01$. With $h_0 = 0.1m$ and $l = 0.12m$ (for the G189 aerofoil) the change $\langle \Delta D \rangle / F_0$ in the theoretical drag coefficient according to Birnbaum's formula is assumed to bc

$$\frac{\langle \Delta D \rangle}{F_0} \cong -1.8 \cdot 10^{-3}\,, \tag{18b}$$

whereas Katzmayr finds an increase in the drag coefficient of about $\langle \Delta D \rangle / F_0 \cong +7.0 \cdot 10^{-3}$ (the two coefficients are not divided by the amplitude of the motion).

Figure 2 shows the amplitudes and phases $\bar{c}_{N,f}$ and $\phi_{N,f}$ for the normal force coefficients and $\bar{c}_{M,f}$ and $\phi_{M,f}$ for the moment coefficients of the plunging (index $f = h$) and pitching (index $f = \alpha$) plate as they are given in [6], [8]. The kinematics in this paper is chosen such that the resulting forces and moments from the numerical solution of the integral equation discussed above (e.g. [13]) agree with the classical results. For the convenience of the reader these functions are provided in the notation of this paper in Appendix A and include the variation of the pitch axis. The coefficients are related to the respective amplitude a by $a = h_0/(l/2)$ for the plunging motion and by $a = \alpha_0$ for the pitching motion; the latter is treated in Chapter 6. Inserting the normal force coefficient in Eq. (18)

$$\langle P \rangle = +\frac{1}{2} h_0\omega \cdot F_0 \cdot \bar{c}_{N,h} \sin \phi_{N,h} \frac{h_0}{l/2} \tag{19}$$

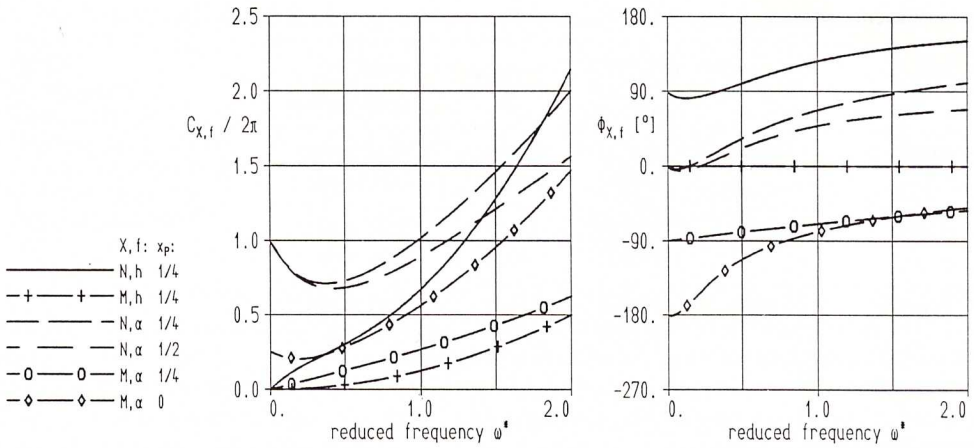

Fig. 2. Amplitudes and phases of normal force and moment coefficients in 2D thin plate theory for plunging and pitching motion versus reduced frequency ω^*

leads with the mean power coefficient $\langle c_\Pi \rangle$ defined by

$$\langle c_\Pi \rangle = \frac{\langle P \rangle}{P_0 a^2}, \qquad P_0 := F_0 \cdot u_0 = \frac{1}{2} \varrho u_0^3 S, \tag{20}$$

to the final result

$$\langle c_\Pi \rangle = \tfrac{1}{2} \omega^* \bar{c}_{N,h} \sin \phi_{N,h} \Rightarrow \langle c_\Pi \rangle \cong \pi \omega^{*2} \quad \text{for} \quad \omega \to 0. \tag{21}$$

From Eq. (A1), Appendix A, the limit $\bar{c}_{N,h} \to 2\pi\omega^*$ for small ω^* is obtained and Figure 2 shows that $\sin \phi_{N,h} \to 1$ holds for $\omega^* \to 0$. Except for 1/2 caused by the mean value formation in Eq. (18) and, of course, a different sign, the same approximate formula as in Eq. (18a) is found. However, the meaning of the expression now is entirely different! The plunging motion requires the mean power $\langle c_\Pi \rangle$ in Eq. (21) over the entire range of ω^* because no other source of energy is available to balance the continuous loss of energy carried away in the wake. From the initial point of time at which the motion begins, the wake grows larger and larger and finally covers a half infinite domain behind the moving obstacle. Thereby, the mean power very soon reaches a constant value and the total kinetic energy in the fluid increases linearly in time. The entry-point of the energy into the mechanical system is the mechanism which drives the plunging motion, e.g. an electric motor, which provides the time-dependent power $P_h(t)$ at the degree of freedom $h(t)$ instead of $g(t)$

$$P_h(t) = -h_0 \omega \sin \omega t \cdot \bar{F}_{z,h} \cos (\omega t + \phi_{z,h}). \tag{22}$$

Eq. (22) is the second contribution to $P(t)$ in Eq. (17). A further conclusion from Eq. (18) is to be drawn. Without details on the power $P_g(t)$ required for the uniform motion

$$P_g(t) = u_0 \cdot \bar{F}_{x,h} \cos (\omega t + \phi_{x,h}), \qquad u_0 = \dot{g}, \tag{23}$$

it is obvious that no mean power $\langle P_g \rangle$ occurs. Hence, neither mean drag nor propulsion is physically possible. Moreover, the investigation of $\bar{F}_{x,h}$ for a very thin profile shows that the values of $\bar{F}_{x,h}$ are zero within the limits of the numerical solution of the corresponding integral equation as long as no steady angle of incidence for a symmetrical profile is assumed. The thin plate solution is the limiting case of vanishing thickness under the same kinematic conditions. The investigation of a profile very close to the thin plate also proves that the presence of a suction force, discussed in the early papers as the basic mechanism for propulsion, is not to be explained on the basis of the linearized theory. Table 1 provides the real and imaginary parts of normal and horizontal force coefficients from the numerical solution for a NACA0001 profile and for comparison the values from the analytical solution (Appendix A) for three typical reduced frequencies ω^* 0.01, 0.1 and 1.0 The accuracy of the numerical solution is $\cong 10^{-4}$).

The " – " means that the value is not to be obtained from the theory. The complex coefficients are related to the forces by

$$\underline{c}_{x,h} = \frac{\underline{F}_{x,h}}{F_0 a_h}, \qquad \underline{c}_{z,h} \equiv \underline{c}_{N,h} = \frac{\underline{F}_{z,h}}{F_0 a_h} \quad \text{with} \quad a_h = \frac{h_0}{l/2}. \tag{24}$$

The normal force coefficient $\underline{c}_{N,h}$ and the coefficient $\underline{c}_{z,h}$ are equivalent to each other.

Table 1. Coefficients of the unsteady forces $\underline{F}_{x,h}$ and $\underline{F}_{z,h}$

ω^*	re $(\underline{c}_{x,h})$ / 2π	im $(\underline{c}_{x,h})$ / 2π	re $(\underline{c}_{z,h})$ / 2π	im $(\underline{c}_{z,h})$ / 2π	wing cross-section
0.01	0.0000	0.0000	0.0004	0.0099	NACA0001
	–	–	0.0004	0.0098	thin plate
0.10	0.0000	0.0000	0.0129	0.0836	NACA0001
	–	–	0.0122	0.0832	thin plate
1.00	0.0000	−0.0000	−0.3969	0.5368	NACA0001
	–	–	−0.3997	0.5394	thin plate

5. Forces and moments

The following linearization equation corresponds to the physical simplifications in the theoretical approach and holds true for the kinematic velocity field of any degree of freedom f

$$v^{*j}_{\mathrm{kin}}(x^{*k}, t) = v^{*j}_{\mathrm{kin},0}(x^{*k}) + \underline{v}^{*j}_{\mathrm{kin},f}(x^{*k}) \cdot \bar{a}_f \cdot \mathrm{e}^{i(\omega t + \psi_f)} . \tag{25}$$

$\bar{a}_f$ is the respective amplitude and ψ_f the prescribed phase shift of the particular degree of freedom with respect to a motion of reference (in this paper the pitching motion has been selected as the motion of reference, hence $\psi_\alpha \equiv 0$). The solution of the integral equation (e.g. [14]) for the induced velocity field provides the relative velocity field $\boldsymbol{v}^*_{\mathrm{rel}}$, formed in the same manner as Eq. (25),

$$v^{*j}_{\mathrm{rel}}(x^{*k}, t) = v^{*j}_{\mathrm{rel},0}(x^{*k}) + \underline{v}^{*j}_{\mathrm{rel},f}(x^{*k}) \cdot \bar{a}_f \cdot \mathrm{e}^{i(\omega t + \psi_f)} . \tag{26}$$

The computation of the complex pressure coefficient requires, due to Bernoulli's equation, the additional knowledge of the complex scalar potential $\Phi(\boldsymbol{x}^*, t)$ for the induced velocity field. A discussion of this aspect is entirely omitted here; the reader is kindly asked to consult the pertinent literature, e.g. [13]–[14]. Unfortunately it is hard to find textbooks or publications providing the complete expressions needed in this paper. The general expression for the pressure coefficient belonging to a particular degree of freedom is

$$c_P(x^{*j}, t) := \frac{p(x^{*j}, t) - p_\infty}{\frac{1}{2}\varrho u_0^2} = \frac{1}{u_0^2}\left(\boldsymbol{v}^{*2}_{\mathrm{kin},f} - \boldsymbol{v}^{*2}_{\mathrm{rel},f} + 2\frac{\partial \Phi_f}{\partial t}\right). \tag{27}$$

p is the local pressure and p_∞ the pressure in the fluid at rest. In the linear approximation the pressure coefficient is formed again like $\boldsymbol{v}^*_{\mathrm{kin}}$ and $\boldsymbol{v}^*_{\mathrm{rel}}$ in Eq. (25) and (26) and reads explicitly

$$c_P(x^{*k}, t) \cong c_{P,0}(x^{*k}) + \underline{c}_{P,f}(x^{*k}) \cdot \bar{a}_f \cdot \mathrm{e}^{i(\omega t + \psi_f)} + [\ldots] \cdot \bar{a}_f^2 \tag{28}$$

with

$$\underline{c}_{P,f}(x^{*k}) = \frac{2}{u_0^2} \cdot (\boldsymbol{v}^*_{\mathrm{kin},0} \cdot \underline{\boldsymbol{v}}^*_{\mathrm{kin},f} - \boldsymbol{v}^*_{\mathrm{rel},0} \cdot \underline{\boldsymbol{v}}^*_{\mathrm{rel},f} + i\omega \cdot \underline{\Phi}_f) \tag{29}$$

and

$$c_{P,0}(x^{*k}) = \frac{1}{u_0^2} \cdot (\boldsymbol{v}^{*2}_{\mathrm{kin},0} - \boldsymbol{v}^{*2}_{\mathrm{rel},0}) . \tag{30}$$

The third summand in brackets proportional to $\bar{a}_f^2$

$$[\ldots] = \frac{1}{u_0^2} \cdot (\underline{\boldsymbol{v}}^{*2}_{\mathrm{kin},f} - \underline{\boldsymbol{v}}^{*2}_{\mathrm{rel},f}) \cdot \mathrm{e}^{2i(\omega t + \psi_f)} \tag{31}$$

has no physical meaning within the limits of a linearized theory because it is merely one of several contributions to the higher order terms of $\bar{a}_f$ occurring in steps previous to the computation of the pressure. As soon as nonlinear terms are regarded in the solution of the integral equation for the "weak" boundary condition, terms containing the squares or higher powers of the amplitude $\bar{a}_f$ have to be considered also (see Appendix B).

Finally, the total pressure coefficient for n degrees of freedom is the sum of the steady pressure coefficient and the contributions from the individual degrees of freedom f and is expressed

$$c_P(x^{*k}, t) = c_{P,0}(x^{*k}) + \sum_{f=1}^{f=n} \underline{c}_{P,f}(x^{*k}) \cdot \bar{a}_f \cdot \mathrm{e}^{i(\omega t + \psi_f)} . \tag{32}$$

The above formula holds true everywhere in the flow field. Computation of the pressure is the necessary prerequisite to obtain the proper expression for the power coefficient. The surface S of a three-dimensional obstacle is considered to be parameterized by a pair (u, v)

$$S = \{x_S^{*k}(u, v) \mid u \in U, v \in V\} . \tag{33}$$

The domains U, V for the parameters are assumed to be defined appropriately. An element $\mathrm{d}S(u, v)$ of the surface is exposed to the force $\mathrm{d}F^{*j}$

$$\mathrm{d}F^{*j} = f^{*j}(x_S^{*k}, t) \cdot \mathrm{d}S(u, v) \tag{34}$$

with the force density f^{*j} defined by the local pressure coefficient

$$f^{*j}(x_S^{*k}, t) = -q_0 \cdot c_P(x_S^{*k}, t) \cdot n_S^{*j}(x_S^{*k}) . \tag{35}$$

n_S^{*j} is the local normal direction of the surface element $\mathrm{d}S$, pointing into the fluid at any point x_S of the body. The minus sign stems from the fact that a positive pressure exerts a force onto the surface and points by definition of the normal vector in a negative direction. In the case of the thin plate solution, the pressure difference $\Delta c_P = c_P^- - c_P^+$ between the pressure c_P^- on the lower side S^- and the pressure c_P^+ on the upper side S^+ is considered (Fig. 3); the minus sign disappears and the force density reads

$$f^{*j}(x_{S^+}^{*k}, t) = +q_0 \cdot \Delta c_P(x_{S^+}^{*k}, t) \cdot n_{S^+}^{*j}(x_{S^+}^{*k}) . \tag{36}$$

Boths elements, the local force density and the kinematic velocity field, are now prepared to form the general expression for the power $P(t)$ in Eq. (16)

$$P(t) = \iint_{S(u,v)} f^{*j}(x_S^{*k}(u, v), t) \cdot v_{\mathrm{kin}}^{*l}(x_S^{*k}(u, v), t) \cdot \delta_{jl} \cdot \mathrm{d}S(u, v) . \tag{37}$$

The power $P(t)$ consists of two parts contributed by the two constituents in the transformation, i.e. translation and rotation. Translation provides the "force" parts

$$P_{\mathrm{trans}}(t) = +\, q_0 \iint_{S(u,v)} c_P(x_S^{*k}(u, v), t) \cdot n_S^{*j}(x_S^{*k}(u, v)) \cdot \dot{a}^{*l}(t) \cdot \delta_{jl} \cdot \mathrm{d}S(u, v) \tag{38}$$

and rotation the "moment" parts

$$P_{\mathrm{rot}}(t) = +q_0 \iint_{S(u,v)} c_P(x_S^{*k}(u, v), t) \cdot n_S^{*j}(x_S^{*k}(u, v)) \cdot x_S^{*m}(u, v)\, \Omega_m^{Tl}(t) \cdot \delta_{jl} \cdot \mathrm{d}S(u, v) . \tag{39}$$

In spite of their different physical meanings, both contributions are treated in Eq. (5) as generalized forces and generalized velocities leading to expressions for the mean powers at the individual degrees of freedom. The different meanings lead to different mechanisms to provide the powers for the mechanical system or to release them. The force parts are related to drag and propulsion and the moment parts to torque oriented clockwise or counterclockwise to the respective moment axis. The next step in the general procedure requires the calculation of the pressure coefficients, then the surface integrals are to be evaluated and, finally, the mean powers according to Eq. (5) are obtained.

Eq. (34) leads to the general expression for the forces acting on a profile

$$F^{*j}(t) = \iint_{S(u,v)} f^{*j}(x_S^{*k}(u, v), t) \cdot \mathrm{d}S(u, v) . \tag{40}$$

Eq. (40) describes the forces with respect to the comoving basis. Obviously, the linearized theory according to Eq. (32) leads to vanishing mean forces $\langle F^{*j} \rangle$. However, F^{*1} and F^{*3} may not be confused with drag and lift. Both physical phenomena are vectorial quantities and act independently of their description with respect to a particular frame of reference. By definition lift points in the opposite direction of the obstacle's weight and, with the motion u_0 perpendicular to the gravity force, drag describes the force of the fluid acting on the moving body parallel to u_0. Dividing the drag into frictional

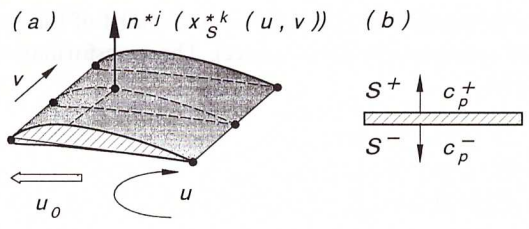

Fig. 3. (a) Normal vector and parameters (u, v) for a wing of finite span, (b) Pressure coefficient $\Delta c_P = c_P^- - c_P^+$ in thin plate theory

and mean dynamic drag, the mean total force on the body

$$\langle \boldsymbol{F}_{\text{body}} \rangle = \langle \boldsymbol{F}_{\text{lift}} \rangle + \boldsymbol{F}_{\text{gravity}} + \boldsymbol{F}_{\text{friction}} + \langle \boldsymbol{F}_{\text{dyn. drag}} \rangle \tag{41}$$

disappears, if mean lift and weight on the one hand, and friction and mean thrust on the other hand, reach a state of equilibrium. $\langle \boldsymbol{F}_{\text{body}} \rangle = 0$ is the condition for the trimmed flight of a body in uniform motion as long as inertial forces are neglected. The occurrence of a trimmed flight is bound to the occurrence of a negative mean dynamic drag, i.e. a mean dynamic thrust, to balance the unavoidable friction. Though friction is also an aerodynamic phenomenon derived from the boundary layer equations, it is useful to destinguish between the steady outward manifestation of friction and the effect of dynamic thrust resulting from unsteady aerodynamics. The aerodynamic forces lift L and drag D are related to the forces F^{*j} by

$$\boldsymbol{F}_{\text{dyn. drag}} + \boldsymbol{F}_{\text{lift}} = D \cdot \boldsymbol{e}_1 + L \cdot \boldsymbol{e}_3 = F^j \boldsymbol{e}_i = F^{*j} \boldsymbol{e}_j^* \tag{42}$$

and read

$$D(t) = F^{*j}(t) \cdot E_j^1(t) \quad \text{and} \quad L(t) = F^{*j}(t) \cdot E_j^3(t) \,. \tag{43}$$

Eq. (43) prepares the definitions of mean drag

$$\langle D \rangle = \frac{1}{T} \int_0^T F^{*j}(t) \cdot E_j^1(t) \, \mathrm{d}t = \frac{1}{T} \int_0^T F^1(t) \cdot \mathrm{d}t \tag{44}$$

and mean lift

$$\langle L \rangle = \frac{1}{T} \int_0^T F^{*j}(t) \cdot E_j^3(t) \, \mathrm{d}t = \frac{1}{T} \int_0^T F^3(t) \cdot \mathrm{d}t \,. \tag{45}$$

The degree of freedom $g(t) = u_0 t$ leads to the mean power $\langle P_g \rangle = u_0 \langle D \rangle$. The same expression is obtained also from Eqs. (16) and (37)

$$P(t) = \iint_S f^{*j}(x_S^{*k}, t) \cdot v_{\text{kin}}^{*l}(x_S^{*k}, t) \cdot E_j^m(t) \cdot E_l^n(t) \cdot \boldsymbol{e}_m \cdot \boldsymbol{e}_n \cdot \mathrm{d}S \,. \tag{46}$$

According to Eq. (10) the contribution in $\boldsymbol{v}_{\text{kin}}^*$ from the translational part of the motion with respect to the basis B is

$$v_{\text{kin, trans}}^n(t) = -\dot{a}^k(t) \cdot E_k^{Tl}(t) \cdot E_l^n(t) = -\dot{a}^n(t) \tag{47}$$

and leads in the formula

$$P_{\text{trans}}(t) = -\dot{a}^n(t) \cdot \iint_S f^m(x_S^{*k}, t) \cdot \delta_{mn} \cdot \mathrm{d}S \tag{48}$$

and for the particular contribution coming from $\dot{a}^1(t) = -g(t)$ to

$$P_g(t) = \dot{g}(t) \cdot F^1(t) \quad \text{with} \quad \langle P_g \rangle = u_0 \cdot \langle D \rangle \,. \tag{49}$$

Eq. (44) permits the important and general conclusion that a necessary condition for the occurrence of mean drag, either positive or negative, is the presence of a time dependent rotation. From linearized theory, no mean propulsion is to be obtained for pure translational degrees of freedom.

The various moments M_f are defined via Eq. (39). The decomposition according to Eq. (5) leads for the respective degree of freedom f to the power

$$P_{\text{rot}, f} = Q_f \cdot \dot{\alpha}_f \quad \text{and} \quad M_f = \delta_f \cdot Q_f \quad \text{with} \quad \delta_f = \pm 1 \,. \tag{50}$$

The plus sign $\delta_f = +1$ holds true for angles α_f defined in a mathematically positive direction (rotation counterclockwise). $\delta_f = -1$ has to be applied for clockwise rotations (mathematically negative).

6. The effects of a pure pitching motion

The pitching motion is confined to a pitch axis perpendicular to the flow and located on the chord of the profile section. The angle of incidence $\alpha(t)$ is oriented in a clockwise direction (mathematically negative). The transformation consists of a translation $a^i(t) = (-g(t), 0, 0)$, $g(t) = u_0 t$, and a rotation with

$$\underline{E}(\alpha(t)) = \begin{bmatrix} \cos\alpha & 0 & -\sin\alpha \\ 0 & 1 & 0 \\ \sin\alpha & 0 & \cos\alpha \end{bmatrix}, \qquad \underline{\Omega}(\alpha(t)) = \begin{bmatrix} 0 & 0 & \dot{\alpha}(t) \\ 0 & 0 & 0 \\ -\dot{\alpha}(t) & 0 & 0 \end{bmatrix}, \tag{51}$$

leading to an intermediate frame of reference B'. The final frame B^* is obtained after another simple transformation shifting o^* away from o' (the intermediate origin) along the x'^1-axis of B' in a negative direction by an amount x_p, i.e. the position of the pitch axis. The corresponding transformation $x'^k = a_p'^k + x^{*j} \cdot \delta_j^k$ is independent of time with $(a_p'^k) = (-x_p, 0, 0)$. Eq. (10) leads to the kinematic velocity field

$$(v_{\text{kin}}^{*j}(x^{*k}, t)) = (\dot{g} \cos \alpha(t) - \dot{\alpha}(t)\, x^{*3},\ 0,\ \dot{g} \sin \alpha(t) + \dot{\alpha}(t)\,(x^{*1} - x_p)) . \tag{52}$$

The angle of incidence may consist of a steady part α_s and an unsteady part $\alpha_i(t) = \alpha_0 \cos \omega t$. The angle $\alpha = \alpha_s + \alpha_i$ is linearized in the unsteady part; the trigonometric addition theorems yield

$$\cos \alpha(t) \cong \cos \alpha_s - \sin \alpha_s \cdot \alpha_i , \qquad \sin \alpha(t) \cong \sin \alpha_s + \cos \alpha_s \cdot \alpha_i . \tag{53}$$

For Δc_P of a thin plate the kinematics in Eq. (52) leads to a simple result. The translational power is connected with the one translational degree of freedom $g(t)$ such that

$$P_{\text{trans}}(t) = +q_0 \cdot \dot{g} \cdot \iint_{S^+} [n_S^{*1}(\cos \alpha_S - \sin \alpha_S \cdot \alpha_i) + n_S^{*3}(\sin \alpha_S + \cos \alpha_S \cdot \alpha_i)] \cdot (\Delta c_{P,0} + \Delta \underline{c}_{P,\alpha}\, \alpha_0\, e^{i\omega t}) \cdot dS \tag{54}$$

and the rotational power belongs to the one rotational degree of freedom $\alpha(t)$ as

$$P_{\text{rot}}(t) = +q_0 \cdot \dot{\alpha} \cdot \iint_{S^+} [-n_S^{*1} x^{*3} + n_S^{*3}(x^{*1} - x_p)] \cdot (\Delta c_{P,0} + \Delta \underline{c}_{P,\alpha}\, \alpha_0\, e^{i\omega t}) \cdot dS . \tag{55}$$

It should be noted that in each step from Eq. (37) to Eqs. (38), (39) and then to Eqs. (54), (55) two minus signs are compensated for and thus result in positive values. The further investigation in this chapter concentrates on the behaviour of the solution for the uncambered thin plate with a steady angle of incidence $\alpha_s = 0$. Before $P_{\text{trans}} = P_g$ and $P_{\text{rot}} = P_\alpha$ are calculated, the values of $\underline{F}_{x,\alpha}$ and $\underline{F}_{z,\alpha}$ are examined.

Table 2. Coefficients of the unsteady forces $\underline{F}_{x,\alpha}$ and $\underline{F}_{z,\alpha}$

ω^*	re $(\underline{c}_{x,\alpha})$ / 2π	im $(\underline{c}_{x,\alpha})$ / 2π	re $(\underline{c}_{z,\alpha})$ / 2π	im $(\underline{c}_{z,\alpha})$ / 2π	wing cross-section
0.01	0.0000	−0.0000	0.9951	−0.0327	NACA0001
	–	–	0.9829	−0.0308	thin plate
0.10	0.0000	−0.0000	0.8516	−0.0454	NACA0001
	–	–	0.8467	−0.0391	thin plate
1.00	0.0000	−0.0000	0.3899	0.9360	NACA0001
	–	–	0.3897	0.9392	thin plate

The complex coefficients are related to the forces by

$$\underline{c}_{x,\alpha} = \frac{\underline{F}_{x,\alpha}}{F_0 \alpha_0}, \qquad \underline{c}_{z,\alpha} \equiv \underline{c}_{N,\alpha} = \frac{\underline{F}_{z,\alpha}}{F_0 \alpha_0} . \tag{56}$$

Table 2 shows that there is almost no difference between the thin plate solution and the very thin but finitely thick profile NACA0001. The $\underline{F}_{x,\alpha}$ again disappear within the accuracy of the numerical solution and may be neglected. In conclusion, the thin plate solution is a good approximation for the forces occurring at profiles with finite thickness. The unsteady normal force and moment coefficients are obtained from the pressure coefficient by

$$\underline{c}_{N,\alpha}(\omega^*, \xi_p) := \frac{1}{S} \cdot \iint_{S^+(u,v)} \Delta \underline{c}_{P,\alpha}(u, v, \omega^*, \xi_p) \cdot dS(u, v) \tag{57}$$

and

$$\underline{c}_{M,\alpha}(\omega^*, \xi_p) := -\frac{1}{S} \cdot \iint_{S^+(u,v)} (\xi - \xi_p) \cdot \Delta \underline{c}_{P,\alpha}(u, v, \omega^*, \xi_p) \cdot dS(u, v) \tag{58}$$

with $\xi := x^{*1}/l$ and $\xi_p := x_p/l$. Both definitions also hold true for the steady normal force and moment coefficients $c_{N,0}$ and $c_{M,0}$. The minus sign in the definition of the moment coefficient is explained in Eq. (50). The dependence on the reduced frequency ω^* and the relative pitch axis ξ_p results from the solution of the corresponding integral equation. Both parameters have been suppressed so far to avoid an annoyingly high number of arguments. For the uncambered thin plate

with $(n_S^{*j}) = (0, 0, 1)$ and with $\alpha_S = 0°$ the powers

$$P_g(t, \omega^*, \xi_p) = q_0 S u_0 \alpha_0 \cos \omega t \cdot [c_{N,0} + \bar{c}_{N,\alpha}(\omega^*, \xi_p)\, \alpha_0 \cos(\omega t + \phi_{N,\alpha}(\omega^*, \xi_p))] \tag{59}$$

and

$$P_\alpha(t, \omega^*, \xi_p) = -q_0 S l(-\alpha_0 \omega) \sin \omega t \cdot [c_{M,0} + \bar{c}_{M,\alpha}(\omega^*, \xi_p)\, \alpha_0 \cos(\omega t + \phi_{M,\alpha}(\omega^*, \xi_p))] \tag{60}$$

lead, through the definition in Eq. (20), to the mean power coefficients

$$\langle c_{\Pi,g}(\omega^*, \xi_p)\rangle = \tfrac{1}{2} \cdot \bar{c}_{N,\alpha}(\omega^*, \xi_p) \cos \phi_{N,\alpha}(\omega^*, \xi_p) \tag{61}$$

and

$$\langle c_{\Pi,\alpha}(\omega^*, \xi_p)\rangle = \tfrac{1}{2} \cdot [-2\omega^* \cdot \bar{c}_{M,\alpha}(\omega^*, \xi_p) \sin \phi_{M,\alpha}(\omega^*, \xi_p)]\,. \tag{62}$$

From the definition of $\langle c_{\Pi,g}\rangle$ it is obvious that the power coefficient is identical to the drag coefficient $\langle c_D\rangle$.

$\langle c_D\rangle \equiv \langle c_{\Pi,g}\rangle > 0$ Dynamic drag occurs (in addition to friction),

$\langle c_D\rangle \equiv \langle c_{\Pi,g}\rangle < 0$ Dynamic propulsion occurs (in the opposite direction of friction).

Fig. 2 shows that a pure pitching motion can effect propulsion. The power needed is raised from the source which drives the pitching motion. This degree of freedom consumes power in the whole range of ω^*, if the pitch axis is $\xi_p = 0.25$. The phase $\phi_{N,\alpha}$ of the normal force coefficient exceeds 90° and $\langle c_{\Pi,g}\rangle$ becomes negative above a reduced frequency $\omega^* \cong 1.6$. The efficiency of the mechanism of propulsion is represented by the ratio between the (negative) mean power gained for propulsion and the power provided for the pitching motion. The remaining power not consumed for propulsion is carried away as kinetic energy in the wake. Defining the efficiency η of the propulsion by

$$\eta(\omega^*, \xi_p) := \frac{-\langle c_{\Pi,g}(\omega^*, \xi_p)\rangle}{\langle c_{\Pi,\alpha}(\omega^*, \xi_p)\rangle} \quad \text{for} \quad \langle c_{\Pi,g}\rangle < 0 \tag{63}$$

the maximum value is $\eta(\omega^*, 0.25) \to 0.5$ for large ω^*. It is worth mentioning that KÜSSNER ([6], p. 419) in this particular case agrees with this paper. The value $\eta(2.0, 0.25) = 0.19$ shows that the efficiency η attainable for reasonable reduced frequencies is very poor. Another peculiarity is the occurrence of negative mean power for the pitching motion in the case of very low reduced frequencies and for $\xi_p = 0.0$. The curve with the diamonds in Figure 2 shows that $\phi_{M,\alpha}(<0.04, 0.0)$ is below $-180°$. The sine in Eq. (62) becomes positive and torsional flutter occurs.

$\langle c_{\Pi,\alpha}\rangle > 0$ Damped torsional motion,

$\langle c_{\Pi,\alpha}\rangle < 0$ Excited torsional motion (torsional flutter).

The effect is well known (e.g. H. W. FÖRSCHING [15], p. 487), but of no major importance in incompressible aerodynamics. As can be seen from Eq. (62), the parameter of stability σ introduced by Försching (his Eq. (6.18) is equivalent to the sine of the phase of the complex moment coefficient $c_{M,\alpha}$.

Finally, Eq. (45) for the mean lift leads to the mean lift coefficient

$$\langle c_{L,\alpha}(\omega^*, \xi_p)\rangle := \frac{\langle L\rangle}{F_0 \cdot \alpha_0^2} = -\frac{1}{2} \cdot [\cos \alpha_s \cdot \bar{c}_{x,\alpha}(\omega^*, \xi_p) \cdot \cos \phi_{x,\alpha}(\omega^*, \xi_p) + \sin \alpha_s \cdot \bar{c}_{z,\alpha}(\omega^*, \xi_p) \cos \phi_{z,\alpha}(\omega^*, \xi_p)]\,. \tag{64}$$

The discussion of $\langle c_{L,a}\rangle$ takes a course similar to $\langle c_{\Pi,\alpha}\rangle$ in Eq. (61). For vanishing $\bar{c}_{x,\alpha}$ and for low reduced frequencies, the mean lift reduces the steady lift for a positive steady angle of incidence and increases the mean lift for $\alpha_S < 0$. The effects are proportional to the square of the pitch amplitude α_0. The influence of α_S is reversed above $\omega^* \cong 1.6$ due to the fact that $\cos \phi_{z,\alpha}$ changes its sign.

7. The interpretation of Katzmayr's experiment

The two observation in Katzmayr's experiment with the pitching profile, increase in drag and decrease in lift for a positive steady angle of incidence (and vice versa), are basic properties of the equations for mean lift and drag, as derived already in the last chapter. Table 3 shows the technical data for those of Katzmayr's experiments discussed here.

The following definitions abbreviate the notation in this chapter

$$\hat{c}_D := \langle \Delta c_{\Pi,\alpha}\rangle \cdot \alpha_0^2 \cdot 10^2 \quad \text{and} \quad \hat{c}_L := \langle \Delta c_{L,\alpha}\rangle \cdot \alpha_0^2 \cdot 10^2\,. \tag{65}$$

The differences are formed between the values for the selected amplitude and $\alpha_0 = 0°$ for the respective angle of incidence. Eqs. (61) and (64) provide a theoretical explanation of the phenomena but the accuracy is unsatisfactory. E.g., for $\alpha_S = 6°$

Table 3. Technical data of Katzmayr's measurements

Profile	G189	Pitch frequency f_z	0.33, 0.5, 0.83 Hz
Chord length l	0.12 m	Reduced frequency ω^*	0.007 ... 0.017
Aspect ratio Λ	6	Pitch axis ξ_P	0.5
Pressure $p_0 = 1/2\varrho u_0^2$	49, 98, 196 Pa	Pitch amplitude α_0	9, 12, 15 deg
Original notation of p_0	5, 10, 20 mm WS	Angle of incidence α_S	0, ± 3, ± 6 deg
$\Rightarrow$ Onset velocity u_0	9.0, 12.7, 17.9 m/s	Plunge frequency f_h	0.19, 0.48 Hz
Reynolds number Re	$7.2 \cdot 10^4$ ... $1.4 \cdot 10^5$	Plunge amplitude h_0	0.1 m

and $\alpha_0 = 15°$ in the linear theory (index lin), $\hat{c}_{D,\mathrm{lin}} \cong 22.0$ overestimates the increase in mean drag and $\hat{c}_{L,\mathrm{lin}} \cong -2.3$ underestimates the decrease in mean lift. For the equivalent experimental configuration (index exp), KATZMAYR ([2], Table 1 on p. 81) finds $\hat{c}_{D,\mathrm{exp}} = 7.2$ and $\hat{c}_{L,\mathrm{exp}} = -20.5$. He mentions that the measurements do not differ for the various frequencies within the tolerance of his measuring device. As far as the dependence on the presure p_0 is concerned, the overall behaviour of $\hat{c}_{D,\mathrm{exp}}$ and $\hat{c}_{L,\mathrm{exp}}$ is also almost independent of p_0 and negligible with respect to the basic interpretation of the results. The theoretical values are obtained from Figure 2. $\bar{c}_{N,\alpha} \cong 2\pi$ and $\phi_{N,\alpha} \cong 0°$ are fairly good approximations for $\omega^* \cong 0.01$. Including the well established formula ([16], p. 13) for the reduction of lift for a wing with finite aspect ratio Λ

$$k(\Lambda) = \frac{\Lambda}{\Lambda + 2}, \quad \text{in the present case} \quad k(6) = \frac{3}{4} \tag{66}$$

leads to a slight reduction of drag, but the discrepancy in lift becomes even worse.

Hitherto the normal force coefficient is assumed to be a linear function of the angle of incidence $c_{N,\mathrm{lin}}(\alpha) \cong 2\pi \cdot \alpha$. No regard is paid to the breakdown of lift above a particular $\alpha \geqq \alpha_1$ due to flow separation which takes place for profiles as well as for the thin plate. Katzmayr's polar curve (Figure 1 in his paper) shows the effect very clearly. The very low reduced frequency permits the assumption that the flow separation on the pitching aerofoil closely follows the polar curve obtained in steady flow. Hence, a more adequate nonlinear theoretical model (index nonl) includes flow separation by means of a modified normal force function $c_{N,\mathrm{nonl}}(\alpha)$. The function approximates flow separation by a parabolic deviation from $c_{N,\mathrm{lin}}$ above the angle of incidence $|\alpha| \geqq \alpha_1$ and with $c_{N,\mathrm{nonl}}(\alpha_1) = c_{N,\mathrm{nonl}}(\alpha_2)$ for another angle of incidence $\alpha_2 > \alpha_1 > 0$. The function is antisymmetric in α, possesses a continuous first derivative and has two extrema $\pm 5/4$. $c_{N,\mathrm{nonl}}(\alpha_1)$ at $\alpha = \pm(\alpha_1 + \alpha_2)/2$

$$\begin{aligned} c_{N,\mathrm{nonl}}(\alpha) &= 2\pi\alpha \quad \text{for} \quad -\alpha_1 \geqq \alpha \leqq \alpha_1 , \\ &= -2\pi\alpha_1 \cdot \left(1 - \frac{\alpha + \alpha_1}{\alpha_1} \cdot \frac{\alpha + \alpha_2}{\alpha_2 - \alpha_1}\right) \quad \text{for} \quad \alpha \leqq -\alpha_1 , \\ &= -2\pi\alpha_1 \cdot \left(1 - \frac{\alpha - \alpha_1}{\alpha_1} \cdot \frac{\alpha - \alpha_2}{\alpha_2 - \alpha_1}\right) \quad \text{for} \quad \alpha \leqq \alpha_1 . \end{aligned} \tag{67}$$

Selecting $\alpha_1 = 8°$ and $\alpha_2 = 20°$, the function approaches fairly well the experimental data in [17], Figure 6.43 on p. 438, up to $\alpha \cong 25°$ and is located slightly below the curve for the lowest Reynolds number $Re = 3.1 \cdot 10^5$. According to Eqs. (44) and (45) mean drag and lift are computed with the linearized $\underline{E}(t)$

$$\begin{aligned} E_3^1(t) &\cong [\sin \alpha_s] + \cos \alpha_s \cdot \alpha_i , \qquad \alpha(t) = \alpha_S + \alpha_0 \cos \omega t , \\ E_3^3(t) &\cong \cos \alpha_s - \sin \alpha_s \cdot \alpha_i , \qquad F^{*3}(t) = F_0 c_{N,\mathrm{nonl}}(\alpha(t)) \cdot k(\Lambda) . \end{aligned} \tag{68}$$

The mean drag is computed without the term in brackets, i.e. no change of the steady drag from the inclined normal force due to $\sin \alpha_S$ is admitted (including the term does not change $\hat{c}_D$ significantly). The results are given in Tables 4a, b and compared with the equivalent data from Katzmayr's experiment for $p_0 = 20$ mm WS ($= 196$ Pa).

Table 4a. Mean drag and lift of the pitching G 189 profile compared to thin plate theory including flow separation; case a: $\alpha_S \geqq 0°$

G 189	$\hat{c}_D$	$\hat{c}_L$	$\hat{c}_D$	$\hat{c}_L$	$\hat{c}_D$	$\hat{c}_L$
$\alpha_0 = 9°$	3.7	0.6	2.5	− 0.6	2.3	− 5.5
12°	6.2	0.0	4.5	− 5.5	3.9	−10.0
15°	8.6	2.3	7.6	− 8.0	7.2	−20.5
Plate	$\hat{c}_D$	$\hat{c}_L$	$\hat{c}_D$	$\hat{c}_L$	$\hat{c}_D$	$\hat{c}_L$
$\alpha_0 = 9°$	5.8	0.0	5.5	− 2.0	4.7	− 7.8
12°	9.7	0.0	9.1	− 6.7	7.4	−16.2
15°	13.4	0.0	12.5	−13.3	10.0	−27.7
	$\alpha_S =$	0°	$\alpha_S =$	+3°	$\alpha_S =$	+6°

For $\alpha_S < 0$ the mean drag for the thin plate remains unaltered and the mean lift changes its sign. Though the model of flow separation for the uncambered thin plate together with the correction for a finite aspect ratio is only a very coarse approximation of the experiment, the tendencies as well as the absolute magnitudes describe the experiment fairly well and are, from the author's point of view, an extremely satisfying interpretation of Katzmayr's experiment with the pitching aerofoil.

Table 4b. Mean drag and lift of the pitching G 189 profile compared to thin plate theory including flow separation; case b: $\alpha_S \leqq 0°$

G 189	$\hat{c}_D$	$\hat{c}_L$	$\hat{c}_D$	$\hat{c}_L$	$\hat{c}_D$	$\hat{c}_L$
$\alpha_0 = 9°$	3.7	0.6	3.9	4.9	5.3	19.7
12°	6.2	0.0	7.2	10.3	8.5	29.8
15°	8.6	2.3	9.5	16.0	10.4	39.2
Plate	$\hat{c}_D$	$\hat{c}_L$	$\hat{c}_D$	$\hat{c}_L$	$\hat{c}_D$	$\hat{c}_L$
$\alpha_0 = 9°$	5.8	0.0	5.5	2.0	4.7	7.8
12°	9.7	0.0	9.1	6.7	7.4	16.2
15°	13.4	0.0	12.5	13.3	10.0	27.7
	$\alpha_S =$	0°	$\alpha_S =$	−3°	$\alpha_S =$	−6°

Not yet interpreted is the plunging motion with its slight increase in drag and a very low decrease in lift. In Chapter 4 it has been proved that the linear theory admits no mean drag and lift for the pure plunging motion. However, for the quasi-steady case of plunging motion, the change of the relative position to the onset flow may be thought of as a pitching motion with an ambiguous pitch axis, the maximum angle of incidence being $\arctan(h_0\omega/u_0) \cong \alpha_0$. Again, for low reduced frequencies $\bar{c}_{N,\alpha} \cong 2\pi$ and $\phi_{N,\alpha} \cong 0°$ holds true independent of the location of the pitch axis. From the mean power $\langle P_g \rangle \cong \pi F_0 \alpha_0^2$ for $\alpha_0 \cong 1°$ the mean drag of the corresponding plunging motion may be estimated from $\langle P_g \rangle \cong \langle D \rangle \cdot \langle h \rangle$ leading to

$$\langle D \rangle = \frac{\langle P_g \rangle}{h_0\omega/\sqrt{2}} = \frac{\sqrt{2}\,\pi F_0 \alpha_0}{u_0} \quad \text{and} \quad \frac{\langle D \rangle}{F_0} = 4.3 \cdot 10^{-3}, \tag{69}$$

which is close to the observed value of $7 \cdot 10^{-3}$. Following the same arguments as above, the very small decrease in lift may be interpreted as a result of Eq. (61).

No attempt is made to also include theoretically the effects of camber and thickness; both investigations are beyond the scope of this paper. The aim of this chapter is to interpret the key results of Katzmayr's outstanding experiment on the basis of unsteady aerodynamics in order to prove the theoretical foundations.

8. The Complementary Mechanisms of Flutter and Propulsion

The basic mechanisms are explained for two-dimensional kinematics. The two-dimensional case (Fig. 4) approximates the three-dimensional spatial motion of an aerodynamic configuration. Figure 5 illustrates the typical degrees of freedom in unsteady aerodynamics and Table 5 shows the denotations in this paper, differing slightly from those frequently used in helicopter dynamics [18].

Table 5. Denotations for corresponding 2D and 3D kinematics

2D motion	3D motion
$g(t) = u_0(t)$ uniform gliding	$g(t) = u_0 t$ uniform gliding
$h(t) = h_0 \cos(\omega t + \varkappa)$ plunging (heaving)	$\vartheta(t) = \vartheta_S + \vartheta_0 \cos(\omega t + \varkappa)$ flapping
$s(t) = s_0 \cos(\omega t + \sigma)$ sliding	$\varphi(t) = \varphi_S + \varphi_0 \cos(\omega t + \sigma)$ lagging
$\alpha(t) = a_S + \alpha_0 \cos \omega t$ pitching	$\alpha(t) = a_S + \alpha_0 \cos \omega t$ feathering
— no equivalent	$\Omega(t) = \Omega_0 t$ uniform rotation

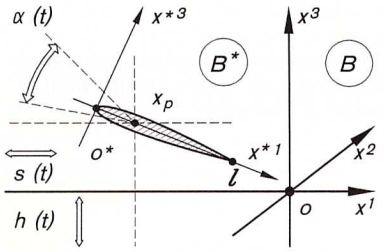

Fig. 4. Three degrees of freedom in two-dimensional kinematics

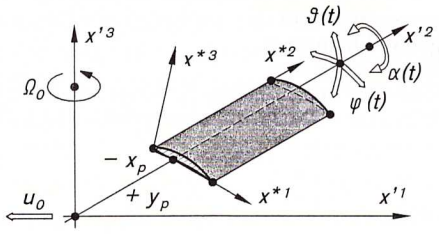

Fig. 5. Typical spatial motions of a three-dimensional wing

Though denoted as 2D kinematics, the set of motions also describes fairly well the degrees of freedom of isolated systems like oscillating engine nacelles suspended from a wing [19]. Including a pitch axis as introduced in Chapter 6, the kinematic velocity field reads in the 2D case

$$\begin{bmatrix} v^{*1}_{\mathrm{kin}}(x^{*k}, t) \\ v^{*2}_{\mathrm{kin}}(x^{*k}, t) \\ v^{*3}_{\mathrm{kin}}(x^{*k}, t) \end{bmatrix} = \begin{bmatrix} \dot{g}\cos\alpha + \dot{s}\cos\alpha - \dot{h}\sin\alpha - \dot{\alpha}x^{*3} \\ 0 \\ \dot{g}\sin\alpha + \dot{s}\sin\alpha + \dot{h}\cos\alpha + \dot{\alpha}(x^{*1} - x_P) \end{bmatrix} \tag{70}$$

the matrix $\underline{E}$ being the same as in Eq. (51). With the linearizations in Eqs. (25) and (53) the following is obtained

$$\begin{aligned} v^{*1}_{\mathrm{kin}} &= (\cos\alpha_S - \alpha_i \sin\alpha_S)\,\dot{g} + \cos\alpha_S \cdot \dot{s} - \sin\alpha_S \cdot \dot{h} - \dot{\alpha} \cdot x^{*3} \\ v^{*3}_{\mathrm{kin}} &= (\sin\alpha_S + \alpha_i \cos\alpha_S)\,\dot{g} + \sin\alpha_S \cdot \dot{s} + \cos\alpha_S \cdot \dot{h} + \dot{\alpha}(x^{*1} - x_P)\,. \end{aligned} \tag{71}$$

For the thin plate the nonzero force density in Eq. (36) reads

$$\begin{aligned} f^{*3}(x^{*1}, t) = q_0 \cdot \Bigg[& \Delta c_{P,0}(x^{*1}) + \Delta c_{P,s}(x^{*1}) \cdot \frac{s_0}{l/2} \cdot \mathrm{e}^{i(\omega t + \sigma)} + \Delta c_{P,h}(x^{*1}) \cdot \frac{h_0}{l/2} \cdot \mathrm{e}^{i(\omega t + \varkappa)} \\ & + \Delta c_{P,\alpha}(x^{*1}) \cdot \alpha_0 \cdot \mathrm{e}^{i\omega t} \Bigg]. \end{aligned} \tag{72}$$

The integral equation for the sliding motion is the same as for the plunging motion, the normal component of $\boldsymbol{v}^*_{\mathrm{kin}}$ multiplied by a tan α_S (cf. Eq. (71)). With the ratio of the sliding motion to the pitching motion τ and the ratio of the plunging motion to the pitching motion λ

$$\tau := \frac{s_0}{\alpha_0 \cdot l/2} \cdot \sin\alpha_S \quad \text{and} \quad \lambda := \frac{h_0}{\alpha_0 \cdot l/2} \cdot \cos\alpha_S \tag{73}$$

the power

$$P(t) = \sum_{f=1}^{f=4} P_f(t) = P_g(t) + P_s(t) + P_h(t) + P_\alpha(t) \tag{74}$$

consists of the contributions

$$\begin{aligned} P_g(t) &= (\sin\alpha_S + \alpha_0 \cos\omega t \cdot \cos\alpha_S) \cdot u_0 \cdot Q(t)\,, \qquad P_s(t) = -\alpha_0 u_0 \omega^* \tau \cdot \sin(\omega t + \sigma) \cdot Q(t)\,, \\ P_h(t) &= -\alpha_0 u_0 \omega^* \lambda \cdot \sin(\omega t + \varkappa) \cdot Q(t)\,, \qquad P_\alpha(t) = +\frac{\alpha_0}{l/2} u_0 \omega^* \cdot \sin\omega t \cdot M(t) \end{aligned} \tag{75}$$

with the functions

$$Q(t) = F_0 \cdot \{c_{N,0} + \alpha_0[\tau \bar{c}_{N,h} \cdot \cos(\omega t + \phi_{N,h} + \sigma) + \lambda \bar{c}_{N,h} \cdot \cos(\omega t + \phi_{N,h} + \varkappa) + \bar{c}_{N,\alpha} \cdot \cos(\omega t + \phi_{N,\alpha})]\} \tag{76}$$

and

$$\begin{aligned} M(t) = F_0 \cdot l \cdot \{ & c_{M,0} + \alpha_0[\tau \bar{c}_{M,h} \cdot \cos(\omega t + \phi_{M,h} + \sigma) + \lambda \bar{c}_{M,h} \cdot \cos(\omega t + \phi_{M,h} + \varkappa) \\ & + \bar{c}_{M,\alpha} \cdot \cos(\omega t + \phi_{M,\alpha})]\}\,. \end{aligned} \tag{77}$$

The contribution from the steady part $c_{N,0}$ in Eq. (76) is not considered, furthermore, its precise computation (including the term v^{*1}_{kin} in Eq. (71)) leads to a vanishing power in the 2D case and to steady induced drag in the 3D case. The total mean power coefficient $\langle c_\Pi \rangle$

$$\langle c_\Pi \rangle = \frac{\langle P \rangle}{P_0 \cdot \alpha_0^2} = \langle c_{\Pi,g} \rangle + \langle c_{\Pi,s} \rangle + \langle c_{\Pi,h} \rangle + \langle c_{\Pi,\alpha} \rangle \tag{78}$$

depends in the 2D case on the parameters given in Table 6.

Table 6. Parameters of the total mean power coefficient $\langle c_\Pi(\omega^*, \xi_p, \lambda, \varkappa, \tau, \sigma, \alpha_S)\rangle$

Reduced frequency	ω^*	Amplitude ratio of sliding to pitching motion	τ
Relative pitch axis	ξ_p	Phase shift of sliding versus pitching motion	σ
Amplitude ratio of plunging to pitching motion	λ	Steady angle of incidence	α_S
Phase shift of plunging versus pitching motion	$\varkappa$		

The coefficients of the individual degrees of freedom in $\langle c_\Pi \rangle$ are

$$\langle c_{\Pi,g}\rangle = +\tfrac{1}{2}\cdot\cos\alpha_S\{\bar{c}_{N,h}[\tau\cos(\phi_{N,h}+\sigma)+\lambda\cos(\phi_{N,h}+\varkappa)]+\bar{c}_{N,\alpha}\cdot\cos\phi_{N,\alpha}\}\,, \tag{79}$$

$$\langle c_{\Pi,s}\rangle = +\tfrac{1}{2}\cdot\omega^*\cdot\tau\{\bar{c}_{N,h}[\tau\sin\phi_{N,h}+\lambda\sin(\phi_{N,h}+\varkappa-\sigma)]+\bar{c}_{N,\alpha}\cdot\sin(\phi_{N,\alpha}-\sigma)\}\,, \tag{80}$$

$$\langle c_{\Pi,h}\rangle = +\tfrac{1}{2}\cdot\omega^*\cdot\lambda\{\bar{c}_{N,h}[\tau\sin(\phi_{N,h}+\sigma-\varkappa)+\lambda\sin\phi_{N,h}]+\bar{c}_{N,\alpha}\cdot\sin(\phi_{N,\alpha}-\varkappa)\} \quad \text{and} \tag{81}$$

$$\langle c_{\Pi,\alpha}\rangle = -\tfrac{1}{2}\cdot 2\omega^*\{\bar{c}_{M,h}[\tau\sin(\phi_{M,h}+\sigma)+\lambda\sin(\phi_{M,h}+\varkappa)]+\bar{c}_{M,\alpha}\cdot\sin\phi_{M,\alpha}\}\,. \tag{82}$$

According to Eq. (64) the coefficient of the mean lift reads

$$\langle c_L\rangle = -\tan\alpha_S\cdot\langle c_{\Pi,g}\rangle\,. \tag{83}$$

The efficiency η of the mechanism of propulsion is the ratio of the power $-\langle c_{\Pi,g}\rangle$, gained to overcome friction to the sum of all other powers released or consumed at the various degrees of freedom executing harmonic (or at least periodic) motions

$$\eta := \frac{-\langle c_{\Pi,g}\rangle}{\langle c_{\Pi,s}\rangle+\langle c_{\Pi,h}\rangle+\langle c_{\Pi,\alpha}\rangle} \quad \text{defined for} \quad \langle c_{\Pi,g}\rangle \leqq 0\,. \tag{84}$$

From the preceding equations several important conclusions are drawn ($\xi_p = 1/4$ and $\cos\alpha_S \cong 1$ are assumed) and subsequently discussed:

The mechanisms of propulsion and flutter require a pitching motion.

The mechanisms of flutter and propulsion are mutually dependent and interchangeable with each other by a mere variation of the reduced frequency as the governing magnitude with respect to unsteady effects.

The limiting case of quasi-steady aerodynamics $\omega^* \to 0$ leads to the mechanism of flutter, not to the mechanism of propulsion, the latter being essentially an effect of unsteady aerodynamics.

Additional mean (positive) lift occurs synchronously with propulsion for a positive steady angle of incidence and mean negative lift for a negative angle (hence, the variation of α_S provides a sensitive lift control).

For low reduced frequencies, the maximum impact of the plunging motion occurs at $\varkappa \cong +90°$ for propulsion as well as for flutter.

A sliding motion with $\sigma \cong \varkappa$ amplifies the impact of the plunging motion.

$\langle c_{\Pi,g}\rangle$ may become negative either by means of a negative $\cos\phi_{N,\alpha}$, requiring $\omega^* \geqq 1.6$ or from $\cos(\phi_{N,h}+\varkappa) \cong -1$ combined with a sufficiently large λ (cf. Fig. 2). The latter case leads to the complementary mechanisms of flutter and propulsion. For simplicity Eqs. (79) and (81) are considered without sliding and for very low reduced frequencies leading to $\langle c_{N,\alpha}\rangle \cong 2\pi$ and $\langle c_{N,h}\rangle \cong 2\pi\cdot\omega^*$. Applying for $\varkappa = 90°$ the trigonometric identities $\cos\phi+\varkappa = -\sin\phi$ and $\sin\phi-\varkappa = -\cos\phi$, the two equations are approximated by

$$\begin{aligned}\langle c_{\Pi,g}\rangle &\cong -\pi(\lambda\omega^*\sin\phi_{N,h}-\cos\phi_{N,\alpha})\,,\\ \langle c_{\Pi,h}\rangle &\cong +\pi\cdot\lambda\omega^*(\lambda\omega^*\sin\phi_{N,h}-\cos\phi_{N,\alpha})\,.\end{aligned} \tag{85}$$

The approximations $\sin\phi_{N,h} \cong 1$ and $\cos\phi_{N,\alpha} \cong 1$ for small ω^* allow a further reduction of the equations

$$\begin{aligned}\langle c_{\Pi,g}\rangle &\cong -\pi(\lambda\omega^*-1)\,,\\ \langle c_{\Pi,h}\rangle &\cong +\pi\cdot\lambda\omega^*(\lambda\omega^*-1)\,.\end{aligned} \tag{86}$$

For a fixed λ the term $\lambda\cdot\omega^*$ may be <1. The plunging motion gains power; the dynamic drag $\langle c_{\Pi,g}\rangle > 0$ usually is compensated for by the much larger thrust of an external engine or – for a sailplane – by the power resulting from the loss of height. Flutter occurs and the fluttering wing of an aeroplane may break off. For a sufficiently large decrease in speed u_0 the reduced frequency increases such that the phenomenon of flutter disappears.

The principal mechanism of animal flight is complementary to the mechanism of flutter. A sufficiently large increase in the reduced frequency for a fixed λ leads to $\lambda\cdot\omega^* > 1$. Thus, the plunging motion continuously requires power to be maintained, coming from the physiological reactions in the muscles of the animal. The gained propulsion $\langle c_{\Pi,g}\rangle < 0$ compensates for the friction of the animal's wings and body.

The limiting case $\omega^* \to 0$ in Eq. (86) leads to the mechanism of flutter with $\langle c_{\Pi,g} \rangle \to \pi$ and $\langle c_{\Pi,h} \rangle \to -\pi\lambda\omega^*$. One might also consider $\lambda \to \infty$, which apparently leads to the mechanism of propulsion, as another limiting case of quasi-steady aerodynamics. The conclusion is a fallacy. Since the amplitude h_0 is limited for physical reasons, $\lambda \to \infty$ has to be achieved by a vanishing amplitude α_0. From Eq. (78) it is obvious that the propulsion itself contains the factor α_0^2. Therefore propulsion vanishes with $\lambda \to \infty$ for a bound amplitude h_0, the efficiency being $\eta \cong 1/\lambda\omega^*$.

The function $G(\alpha_0)$

$$G(\alpha_0) = \frac{1}{2} \cdot (\alpha_0 \cdot g_1 + \alpha_0^2 \cdot g_2) \quad \text{with} \quad g_1 = \frac{h_0}{l/2} \cdot \bar{c}_{N,h} \cos(\phi_{N,h} + \varkappa) \quad \text{and} \quad g_2 = \bar{c}_{N,\alpha} \cdot \cos \phi_{N,\alpha} \tag{87}$$

for the mean drag coefficient $G(\alpha_0) = \langle D \rangle / F_0$ (including the amplitude) has an extremum for $\hat{\alpha}_0 = -g_1/2g_2$ with $G(\hat{\alpha}_0) = -g_1^2/8g_2$. For low reduced frequencies the extremum is the maximum propulsion $F_0 \cdot G(\hat{\alpha}_0)$, i.e., the negative minimum drag. The corresponding $\hat{\lambda} \cong 2/\omega^*$ leads to large values for $\omega^* \to 0$ accompanied by $\eta \cong 1/2$.

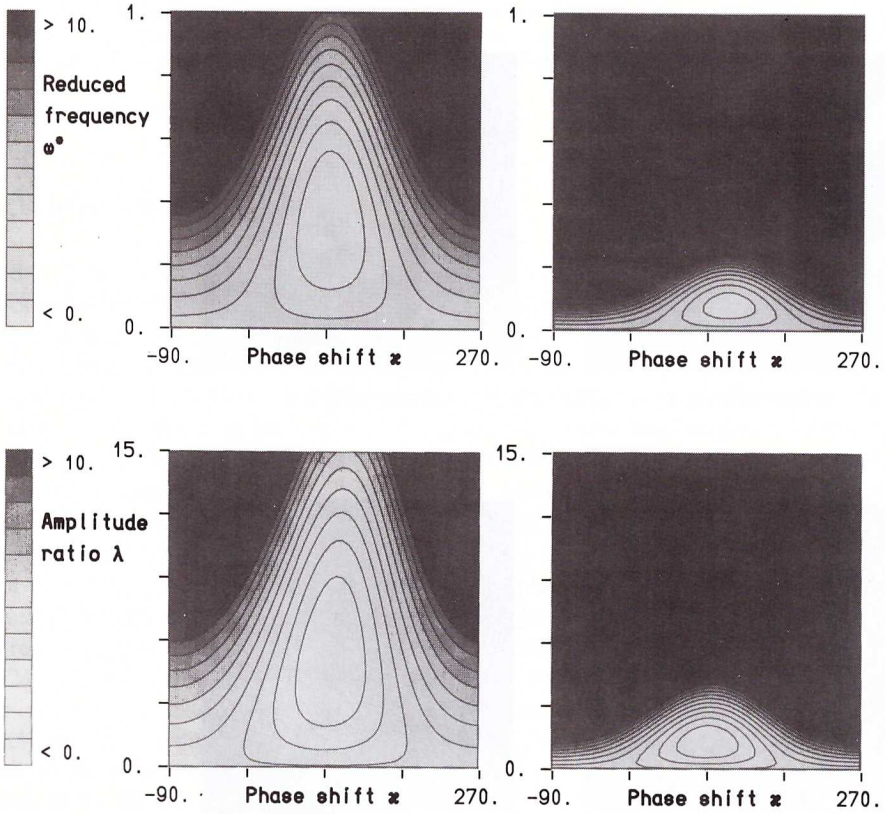

Fig. 6a, b. Total mean power coefficient $\langle c_\Pi \rangle$ for two amplitude ratios $\lambda = 3$ (left) and $\lambda = 12$ (right) and for two reduced frequencies $\omega^* \doteq 0.2$ (left) and $\omega^* = 1.0$ (right); reduced frequency ω^* versus phase shift $\varkappa$ (top) and amplitude ratio λ versus phase shift $\varkappa$ (bottom)

Figures 6a–b illustrate that the dependence between reduced frequency and amplitude ratio is almost the same for an appropriate scale. The total mean power coefficients for ω^* versus $\varkappa$ and λ versus $\varkappa$ only differ slightly; this holds true for all coefficients in Eqs. (79)–(82). The scale of the contour plots is given on the left hand side of each figure. Fig. 7 shows the efficiency η in Eq. (84) for two reduced frequencies $\omega^* = 0.2$ and 1.0 for plunging and pitching motion (without sliding). Whereas in the first case the efficiency exceeds 0.8, in the second case the maximum falls below 0.6 and decreases rapidly for even higher reduced frequencies. The figure is the most important one of the paper with respect to animal flight and illustrates that the propulsion of animals is an inherent and basis property of the theory of unsteady aerodynamics. For any reduced frequency, animal flight is restricted to certain well defined and narrow areas of the governing parameters representing a compromise between optimum efficiency and the necessary propulsion to overcome the unavoidable frictional drag. In Figures 8a–c the power coefficients for the three degrees of freedom g, h and α are plotted. Maximum efficiency is very close to vanishing propulsion; i.e., the less friction to be overcome by propulsion, the more efficient the mechanism of propulsion is. The disadvantage of low reduced frequencies is that animals operating in this regime have to be optimized perfectly for low drag or they waste too much of their input energy in comparison to animals operating at higher reduced frequencies, where the slope of decreasing efficiency is less steep than for a very low reduced frequency.

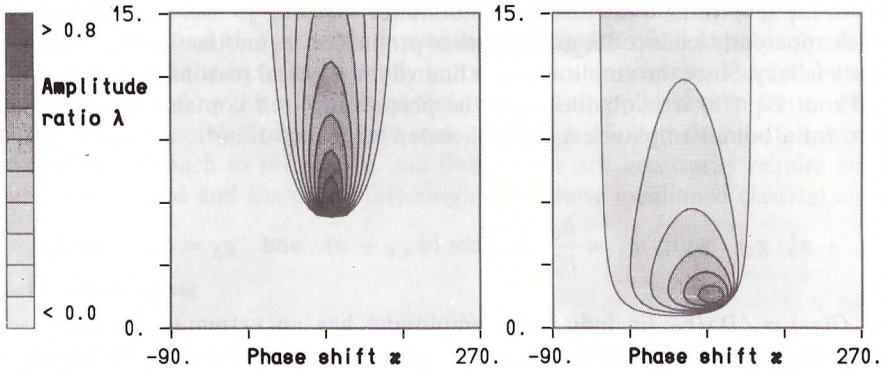

Fig. 7. Efficiency η for two reduced frequencies $\omega^* = 0.2$ (left) and $\omega^* = 1.0$ (right); amplitude ratio λ versus phase shift $\varkappa$

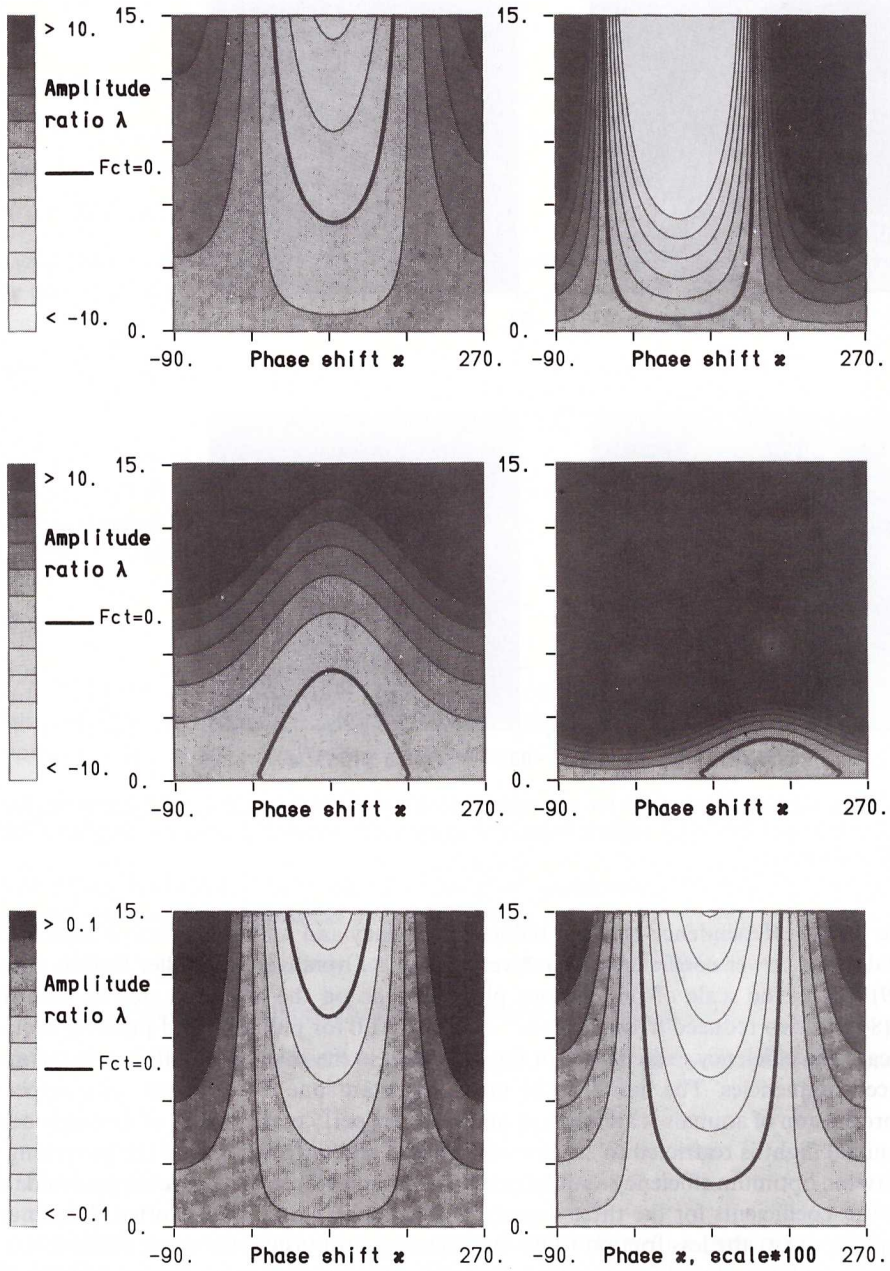

Fig. 8a–c. Mean power coefficients for two reduced frequencies $\omega^* = 0.2$ (left) and $\omega^* = 1.0$ (right) and for amplitude ratio λ versus phase shift $\varkappa$; $\langle c_{\Pi,g} \rangle$ (top), $\langle c_{\Pi,h} \rangle$ and $\langle c_{\Pi,\alpha} \rangle$(bottom)

Recent preliminary comparisons between the theoretical description presented in this paper and results from W. Zarnack's observation of the kinematics of insects ([20], [21]) seem to indicate that the lines of zero $\langle c_{\Pi,s}\rangle$ and $\langle c_{\Pi,\alpha}\rangle$ play an important role. At least the animals observed, Locusta migratoria L., tend to have phase shifts $\varkappa$, σ and amplitude ratios λ, τ very close to these lines. The basic relations of possible relevance for a detailed interpretation of animal flight are illustrated in Fig. 9. For the very typical values $\lambda = 12$, $\tau = 6$, and $\omega^* = 0.2$ the contour plots of $\langle c_{\Pi,s}\rangle$ and $\langle c_{\Pi,\alpha}\rangle$ for σ versus $\varkappa$ show that the zero-lines intersect at distinct points $(\varkappa_0, \sigma_0)$ in the centre of the figure coinciding very closely with the observations. The preceding example also demonstrates the capability of the theoretical approach to represent complex features in animal flight.

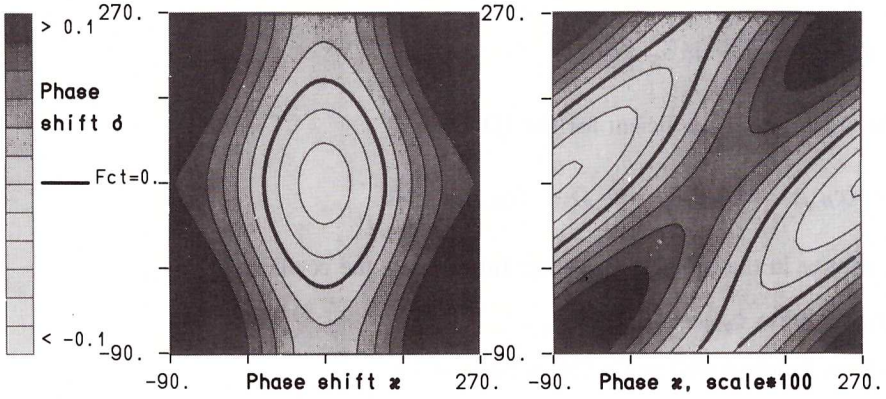

Fig. 9. Mean power coefficients $\langle c_{\Pi,\alpha}\rangle$ (left) and $\langle c_{\Pi,s}\rangle$ (right) for $\omega^* = 0.2$, $\lambda = 12$ and $\tau = 6$; phase shift σ versus phase shift $\varkappa$

9. Computation for three-dimensional kinematics

Excluding the uniform rotation preferably applied in approximative computations of unsteady pressures for rotary wings and omitting the offset y_p for the hinge (Fig. 5), the transformation

$$e_j^* = E_j^i(\vartheta(t), \varphi(t), \alpha(t))\, e_i \tag{88}$$

by the matrix $\underline{E}(t)$ for 3D kinematics according to Table 5 reads explicitly:

$$\begin{bmatrix} e_1^* \\ e_2^* \\ e_3^* \end{bmatrix} = \begin{bmatrix} \cos\alpha & 0 & -\sin\alpha \\ 0 & 1 & 0 \\ \sin\alpha & 0 & \cos\alpha \end{bmatrix} \cdot \begin{bmatrix} \cos\varphi & \sin\varphi & 0 \\ -\sin\varphi & \cos\varphi & 0 \\ 0 & 0 & 1 \end{bmatrix} \cdot \begin{bmatrix} 1 & 0 & 0 \\ 0 & \cos\vartheta & -\sin\vartheta \\ 0 & \sin\vartheta & \cos\vartheta \end{bmatrix} \cdot \begin{bmatrix} e_1 \\ e_2 \\ e_3 \end{bmatrix}. \tag{89}$$

The matrix

$$\underline{E}(\vartheta(t), \varphi(t), \alpha(t)) = \begin{bmatrix} \cos\varphi\cos\alpha & -\sin\vartheta\sin\alpha + \cos\vartheta\sin\varphi\cos\alpha & -\cos\vartheta\sin\alpha - \sin\vartheta\sin\varphi\cos\alpha \\ -\sin\varphi & \cos\vartheta\cos\varphi & -\sin\vartheta\cos\varphi \\ \cos\varphi\sin\alpha & \sin\vartheta\cos\alpha + \cos\vartheta\sin\varphi\sin\alpha & \cos\vartheta\cos\alpha - \sin\vartheta\sin\varphi\sin\alpha \end{bmatrix} \tag{90}$$

leads to

$$\underline{\Omega}(\vartheta(t), \varphi(t), \alpha(t)) = \begin{bmatrix} 0 & -\omega^3 & \omega^2 \\ \omega^3 & 0 & -\omega^1 \\ -\omega^2 & \omega^1 & 0 \end{bmatrix} \quad \text{with} \quad \begin{bmatrix} \omega^1 \\ \omega^2 \\ \omega^3 \end{bmatrix} = \begin{bmatrix} -\dot\vartheta\cos\varphi\cos\alpha - \dot\varphi\sin\alpha \\ \dot\vartheta\sin\varphi + \dot\alpha \\ -\dot\vartheta\cos\varphi\sin\alpha + \dot\varphi\cos\alpha \end{bmatrix}. \tag{91}$$

Including the pitch axis x_p as in Chapter 6 the kinematic velocity field is:

$$\begin{bmatrix} v_{\text{kin}}^{*1}(x^{*k}, t) \\ v_{\text{kin}}^{*2}(x^{*k}, t) \\ v_{\text{kin}}^{*3}(x^{*k}, t) \end{bmatrix} = \begin{bmatrix} \dot g\cos\alpha\cos\varphi + \dot\varphi x^{*2}\cos\alpha - \dot\vartheta x^{*2}\sin\alpha\cos\varphi - \dot\alpha x^{*3} - \dot\vartheta x^{*3}\sin\varphi \\ -\dot\varphi[(x^{*1} - x_P)\cos\alpha + x^{*3}\sin\alpha] + \dot\vartheta[(x^{*1} - x_P)\cos\varphi\sin\alpha - x^{*3}\cos\varphi\cos\alpha] \\ \dot g\sin\alpha\cos\varphi + \dot\varphi x^{*2}\sin\alpha + \dot\vartheta x^{*2}\cos\alpha\cos\varphi + \dot\alpha(x^{*1} - x_P) + \dot\vartheta(x^{*1} - x_P)\sin\varphi \end{bmatrix}. \tag{92}$$

The nonzero v_{kin}^{*2} indicates the presence of centrifugal forces caused by flapping ($\dot\vartheta$) and lagging ($\dot\varphi$) motion. Linearizing $\vartheta(t)$ and $\varphi(t)$ according to Eq. (25) and analogously to Eq. (53) it is obtained for the normal component of $\boldsymbol{v}_{\text{kin}}^*$

$$\begin{aligned} v_{\text{kin}}^{*3} = {} & (\sin\alpha_S \cdot \cos\varphi_S + \alpha_i \cdot \cos\alpha_S \cdot \cos\varphi_S - \varphi_i \cdot \sin\alpha_S \cdot \sin\varphi_S)\,\dot g \\ & + \sin\alpha_S \cdot \dot\varphi \cdot x^{*2} + \cos\alpha_S \cdot \cos\varphi_S \cdot \dot\vartheta \cdot x^{*2} + \dot\alpha(x^{*1} - x_P) + \dot\vartheta \cdot (x^{*1} - x_P)\sin\varphi_S\,. \end{aligned} \tag{93}$$

For $\varphi_S = 0°$ the expressions for v_{kin}^{*3} in Eq. (93) and v_{kin}^{*3} in Eq. (71) show almost complete conformity. The local $\dot{\vartheta} \cdot x^{*2}$ corresponds to $\dot{h}$ and $\dot{\varphi} \cdot x^{*2}$ corresponds to $\dot{s}$. Hence, the 3D case is very reasonably approximated by the 2D coefficients of forces and moments and a spanwise integration of x^{*2}, the local amplitudes being $h_0 = x^{*2} \tan \vartheta_0$ and $s_0 = x^{*2} \tan \varphi_0$ (strip theory). The case $\varphi_S \neq 0°$ is treated similarly leading to sightly different definitions of the ratios λ and τ compared to Eq. (73). With b being the span of the (rectangular) 3D wing, the ratios are

$$\tau := \frac{\varphi_0 \cdot b/2}{\alpha_0 \cdot l/2} \cdot \sin \alpha_S \quad \text{and} \quad \lambda := \frac{\vartheta_0 \cdot b/2}{\alpha_0 \cdot l/2} \cdot \cos \alpha_S \cdot \cos \varphi_S \,. \tag{94}$$

The last summand in Eq. (93) and the term with φ_i belonging to $\dot{g}$ require the definition of two further ratios χ and ψ

$$\chi := \frac{\vartheta_0}{\alpha_0} \cdot \sin \varphi_S \quad \text{and} \quad \psi := \frac{\varphi_0}{\alpha_0} \cdot \sin \alpha_S \cdot \sin \varphi_S \,. \tag{95}$$

The various coefficients in the mean power coefficient for the 3D case

$$\langle c_\Pi \rangle = \frac{\langle P \rangle}{P_0 \cdot \alpha_0^2} = \langle c_{\Pi,g} \rangle + \langle c_{\Pi,\varphi} \rangle + \langle c_{\Pi,\vartheta} \rangle + \langle c_{\Pi,\alpha} \rangle \,, \tag{96}$$

as defined in Eqs. (79)–(82), change in the following manner: Introducing the coefficients

$$\mathfrak{c}_{N,\eta} := (i\omega^*)^{-1} \cdot \mathfrak{c}_{N,h} \quad \text{and} \quad \mathfrak{c}_{N,\xi} := \mathfrak{c}_{N,\alpha} - \mathfrak{c}_{N,\eta} \,, \tag{97}$$

the last term with $\bar{c}_{N,\alpha}$ in the force function $Q(t)$ in Eq. (76) is replaced by

$$\cos \alpha_S \cos \varphi_S \bar{c}_{N,\eta} \cdot \cos (\omega t + \phi_{N,\eta}) + \bar{c}_{N,\xi} \cdot \cos (\omega t + \phi_{N,\xi}) \tag{97a}$$

and the function is extended by

$$Q(t) = \ldots + F_0 \cdot \alpha_0 \chi \bar{c}_{N,\xi} \cdot \cos (\omega t + \phi_{N,\xi} + \varkappa) - F_0 \cdot \alpha_0 \psi \bar{c}_{N,\eta} \cdot \cos (\omega t + \phi_{N,\eta} + \sigma) \,. \tag{98}$$

The moment function $M(t)$ in Eq. (77) is treated in the same way replacing all subscripts N simultaneously by M.

Explicitly altered are the first and the last power function in Eq. (75)

$$\begin{aligned} P_g(t) &= [\sin \alpha_S \cos \varphi_S + \alpha_0 (\cos \alpha_S \cdot \cos \varphi_S \cdot \cos \omega t - \psi \cos (\omega t + \sigma))] \cdot u_0 \cdot Q(t) \,, \\ P_\alpha(t) &= + \frac{\alpha_0}{l/2} u_0 \omega^* \cdot (\sin \omega t + \chi \cdot \cos (\omega t + \varkappa)) \cdot M(t) \,, \end{aligned} \tag{99}$$

leading in Eq. (96) to expressions similar to Eqs. (79)–(82).

10. Concluding remarks

The present paper outlines the basic and inherent properties of the theory of unsteady aerodynamics with respect to flutter and propulsion, using the balance of mechanical energy as the guiding principle. Both mechanisms are explained as complementary processes depending on the various parameters of the kinematic motion and particularly on the reduced frequency as the governing magnitude with respect to unsteady effects. Camber and thickness may improve the efficiency of propulsion, but they are not a prerequisite for propulsion to take place. However, all equations for forces and moments are derived such that both tools for improving the thin plate theory can easily be included. Though the two-dimensional theory already comprises a complete model for flutter and propulsion, the theory is also capable of including three-dimensional effects and spatial configurations like engine nacelles, the author's current subject of research.

It is beyond the scope of the paper to compare the theory with the numerous measurements within the decades following Katzmayr's very first experiment in unsteady aerodynamics. The experiments and measurements of E. VON HOLST and D. KÜCHEMANN with mechanical models of flying animals ([22]–[24]) are not to be explained on the basis of their quasi-steady theory. In [23], p. 282, they write:

> The given force coefficients $\bar{c}_a$, $\bar{c}_w$ and $\bar{c}_s$ (in a preceding table) have not been obtained from the quasi-steady theory, but have been taken from the conditions of equilibrium for the steady climbing flight and from the power of the engine (twisted-rubber engine), assuming an estimated efficiency η of 0.5 due to losses in the gear box etc.

A careful check has proved that von Holst's model does not only fly in reality but also on the basis of the theory in this paper, the reduced frequency being $\omega^* \simeq 0.4$. Various other experiments prove the capability of the theory for explaining the significant measurements of animal flight, particularly the very detailed observations of W. ZARNACK ([25], [26]) on locust flight within the last two decades. The wings of insects very much resemble thin plates, the shape remaining almost unaltered during flight and thus providing a very suitable subject for comparison with simple theoretical models.

Acknowledgement

The author is obliged to Dr. BUBLITZ for generously supplying his notes and documents, to his collegues at the "DLR-Institut für Aeroelastik" and also at the "Max-Planck-Institut für Strömungsforschung" for many fruitful discussions and, last but not least, to Prof. ZARNACK at the "1. Zoologisches Institut der Universität Göttingen" for the close cooperation within recent years and his continuous encouragement to elaborate this paper.

References

1 BUBLITZ, P.: Geschichte der Entwicklung der Aeroelastik in Deutschland von den Anfängen bis 1945. DFVLR-Mitt. **86—25**. Wiss. Berichtswesen der DFVLR, Köln 1986.
2 KATZMAYR, R.: Über das Verhalten von Flügelflächen bei periodischen Änderungen der Geschwindigkeitsrichtung. Z. f. Flugtechnik und Motorluftschiffahrt **6** (1922), 80—82; and KATZMAYR, R., Effect of periodic changes of angle of attack on behavior of airfoils. N.A.C.A.T.M. No. **147** (1922).
3 MUNK, M.; HÜCKEL, E.: Der Profilwiderstand von Tragflügeln. Techn. Ber. Flugzeugmeisterei **II** (1918), 451—461.
4 NACHTIGALL, W.: Warum die Vögel fliegen. Rasch und Röhring Verlag, Hamburg/Zürich 1985.
5 BIRNBAUM, W.: Das ebene Problem des schlagenden Flügels. ZAMM **4** (1924), 277—292.
6 KÜSSNER, H. G.: Zusammenfassender Bericht über den instationären Auftrieb von Flügeln. Luftfahrtforschung **13** (1936), 410—424.
7 GARRICK, I. E.: Propulsion of a flapping and oscillating airfoil. N.A.C.A. Report No. **567** (1936).
8 THEODORSEN, TH.: General theory of aerodynamic instability and the mechanism of flutter. N.A.C.A. Report No. **496** (1935).
9 WAGNER, H.: Über die Entstehung des dynamischen Auftriebs von Tragflügeln. ZAMM **5** (1925), 17—35.
10 LICHNEROWICZ, A.: Einführung in die Tensoranalysis. Bibliograph. Institut AG, Mannheim 1966.
11 SEND, W.: Zur Theorie des Rotorblattes in inkompressibler Strömung (I). DFVLR IB **253—78** J **10**, Göttingen 1978.
12 SEND, W.: Analytical representation of the three-dimensional wake integral in unsteady flow. Proc. of the Colloquium Honoring Hans Georg Küssner on the Occasion of his 80th Birthday. Göttingen 1980.
13 SEND, W.: Higher-order panel method applied to vorticity-transport equation. Fifth European Rotorcraft and Powered Lift Aircraft Forum. No. **16**. Amsterdam 1979.
14 SEND, W.: Der instationäre Nachlauf hinter schlanken Auftriebskörpern in inkompressibler Strömung. ZAMM **64** (1984), 7—15.
15 FÖRSCHING, H. W.: Grundlagen der Aeroelastik. Springer-Verlag, Berlin/Heidelberg/New York 1974.
16 SCHLICHTING, H.; TRUCKENBRODT, E.: Aerodynamik des Flugzeugs. Band II. Springer-Verlag, Berlin/Heidelberg/New York 1969.
17 SCHLICHTING, H.; TRUCKENBRODT, E.: Aerodynamik des Flugzeugs. Band I. Springer-Verlag, Berlin/Heidelberg/New York 1959
18 BRAMWELL, A. R. S.: Helicopter dynamics. Edward Arnold Publ., London 1976.
19 SEND, W.: Forces and moments of an engine nacelle. In: Proceedings of the European Forum on Aeroelasticity and Structural Dynamics 1989. DGLR Bericht **89—1**, Bonn 1989.
20 SCHWENNE, TH.; ZARNACK, W.: Movement of the hindwings of Locusta migratoria, measured with miniature coils. J. comp. Physiol. A **160** (1987), 657—666.
21 ZARNACK, W.: The effect of forewing depressor activity on wing movement during locust flight. Biol. Cybern. **58** (1978), 661—676.
22 VON HOLST, E.: Über „künstliche Vögel" als Mittel zum Studium des Vogelflugs. J. f. Ornithologie **91** (1943), 406—447.
23 KÜCHEMANN, D.; VON HOLST, E.: Zur Aerodynamik des Tierflugs. Luftwissen **8** (1941), 277—282.
24 VON HOLST, E.: Untersuchungen zur Flugbiophysik I. Messungen zur Aerodynamik kleiner schwingender Flügel. Biol. Zentralblatt **63** (1943), 289—326.
25 ZARNACK, W.: Flugbiophysik der Wanderheuschrecke Locusta migratoria L. I. Die Bewegungen der Vorderflügel. J. comp. Physiol. **78** (1972), 356—395.
26 ZARNACK, W.: Untersuchungen zum Flug der Wanderheuschrecken. Die Bewegungen, räumlichen Lagebeziehungen sowie Formen und Profile von Vorder- und Hinterflügeln. In: NACHTIGALL, W. (ed.): BIONA-Report 1. Gustav Fischer Verlag, Stuttgart/New York 1983.
27 ABRAMOWITZ, M.; STEGUN, I. A. (ed.): Handbook of mathematical functions. Dover Publications, New York 1965.
28 FUNG, Y. C.: The theory of aeroelasticity. Dover Publications, New York 1969.
29 STEPHEN, E.; KEDZIE, CH.; ROBINSON, M. C.: Unsteady pressure loads from plunging aerfoils. Paper AIAA-89-2228-CP, 1989.

Received January 3, 1990

Address: Dr. rer. nat. WOLFGANG SEND, DLR-Institut für Aeroelastik, Bunsenstraße 10, W-3400 Göttingen, Germany

Appendix A

Normal force and moment coefficients of the plunging and pitching thin plate (2D):

$$c_{N,h}(\omega^*) = 2\pi \cdot [i\omega^* C(\omega^*) - \tfrac{1}{2}\omega^{*2}], \tag{A1}$$

$$c_{M,h}(\omega^*, \xi_P) = c_{M,h}(\omega^*, \tfrac{1}{4}) + (\xi_P - \tfrac{1}{4}) \cdot c_{N,h}(\omega^*) \quad \text{with}$$
$$c_{M,h}(\omega^*, \tfrac{1}{4}) = -2\pi \cdot [-\tfrac{1}{8}\omega^{*2}], \tag{A2}$$

$$c_{N,\alpha}(\omega^*, \xi_P) = c_{N,\alpha}(\omega^*, \tfrac{1}{4}) - 2(\xi_P - \tfrac{1}{4}) \cdot c_{N,h}(\omega^*) \quad \text{with}$$
$$c_{N,\alpha}\left(\omega^*, \frac{1}{4}\right) = 2\pi \cdot \left[C(\omega^*) \cdot (1 + i\omega^*) + \frac{i}{2}\omega^* - \frac{1}{4}\omega^{*2}\right], \tag{A3}$$

$$\varsigma_{M,\alpha}(\omega^*, \xi_P) = \varsigma_{M,\alpha}\left(\omega^*, \frac{1}{4}\right) - 2\left(\xi_P - \frac{1}{4}\right) \cdot \varsigma_{M,h}(\omega^*, 1/4) + \left(\xi_P - \frac{1}{4}\right) \cdot \varsigma_{N,\alpha}\left(\omega^*, \frac{1}{4}\right) - 2 \cdot \left(\xi_P - \frac{1}{4}\right)^2 \cdot \varsigma_{N,h}(\omega^*),$$

$$\varsigma_{M,\alpha}\left(\omega^*, \frac{1}{4}\right) = -2\pi \cdot \left[\frac{i}{4}\,\omega^* - \frac{3}{32}\,\omega^{*2}\right], \tag{A4}$$

$$C(\omega^*) = \frac{H_1^{(2)}(\omega^*)}{H_1^{(2)}(\omega^*) + i \cdot H_0^{(2)}(\omega^*)}. \tag{A5}$$

The function $C(\omega^*)$ is called Theodorsen's function, where $H_\nu^{(2)}$ is the Hankel function of order ν [27]. Approximations of the function $C(\omega^*)$ by simple algebraic expressions are discussed in [28], p. 215.
KÜSSNER's coefficients k_a, k_b and m_a, m_b in [6], Eq. 42, are related to the preceding functions by

$$\varsigma_{N,h}(\omega^*) = \pi \cdot k_a, \qquad \varsigma_{M,h}(\omega^*, 1/4) = -\frac{\pi}{2} \cdot m_a,$$

$$\varsigma_{N,\alpha}(\omega^*, 1/4) = \pi \cdot k_b, \qquad \varsigma_{M,\alpha}(\omega^*, 1/4) = -\frac{\pi}{2} \cdot m_b. \tag{A6}$$

Changing the pitch axis from an arbitrary x_{P1} to another x_{P2} leads to the additional term $-\dot{\alpha}(\chi_{P2} - x_{P1})$ in Eq. (71), to be interpreted as an additional "plunging motion" $h_P(t) = h_{0P} \cos(\omega t + \psi_P)$ with the amplitude $h_{0P} = \alpha_0(x_{P2} - x_{P1})$ and the phase shift $\psi_P = \pi$. Selecting $x_{P1}/l = 1/4$ and $\xi_P = x_{P2}/l$ and including the additional term $h_P(t)$ the recalculation of normal force and moment coefficients leads to Eqs. (A1)–(A4).

Appendix B

Recently published results from unsteady pressure measurements [29] demand further theoretical investigations of nonlinear contributions to mean forces. Basically, the nonlinear terms of Bernoulli's equation in Eq. (31) could interpret the observed drag reduction for a plunging motion. However, the measured effect converts for a slight increase of the steady angle of incidence α_S ($\alpha_S > 5°$) to a drastic increase in mean drag being unpredictable within the theoretical limits. Furthermore, the assumed linear vorticity transport in the theoretical model does not convect changes of the energy balance at the profile (from included nonlinear terms) into the fluid, if these do not originate from the solution of the corresponding integral equation.